Differential Magnetometry

Selective magnetometry for in vivo use

Sebastiaan Waanders

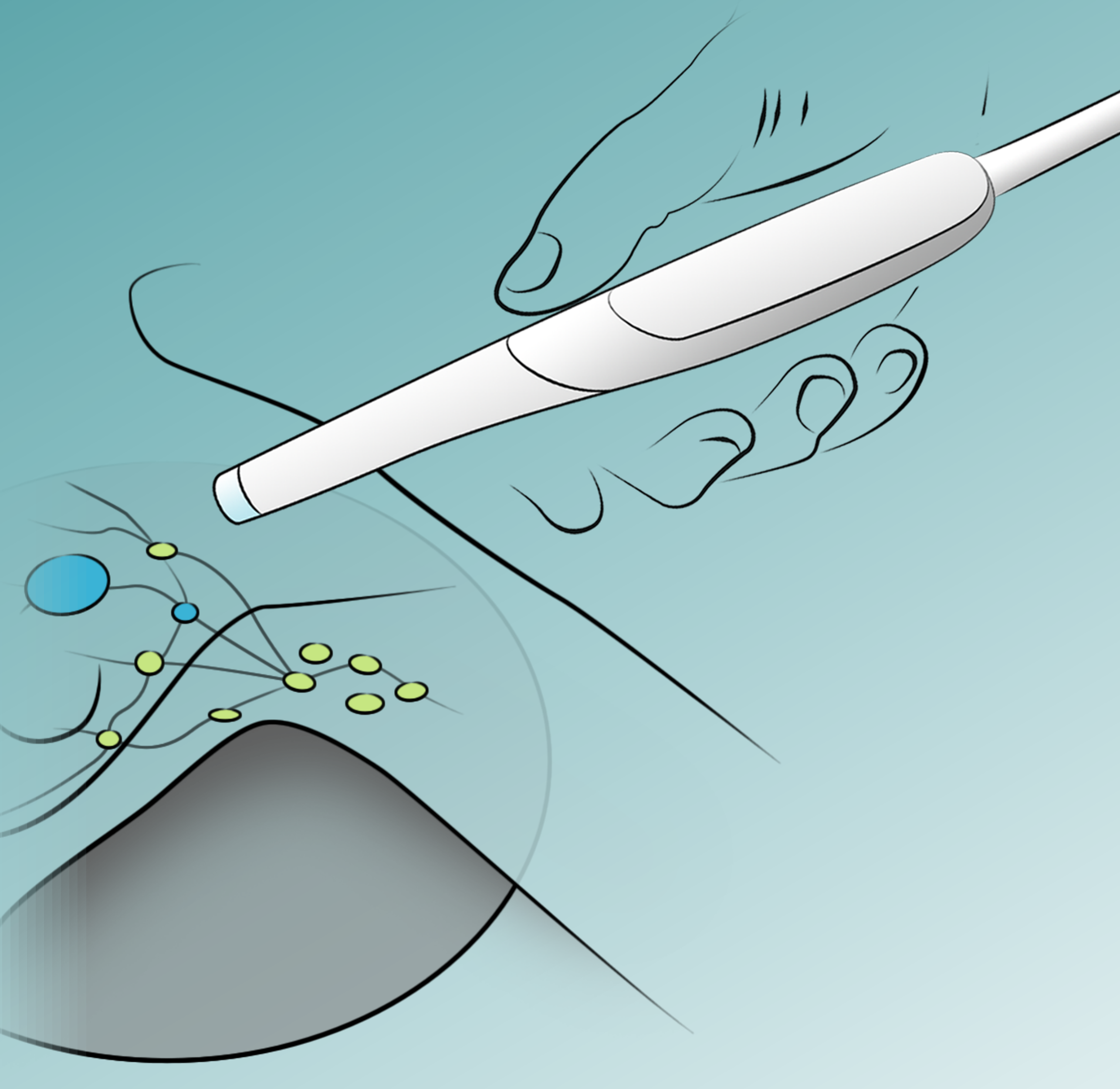

Differential Magnetometry
Selective magnetometry for in vivo use

S. Waanders

DIFFERENTIAL MAGNETOMETRY
SELECTIVE MAGNETOMETRY FOR IN VIVO USE

DISSERTATION

to obtain
the degree of doctor at the University of Twente,
on the authority of the rector magnificus,
prof. dr. ir. A. Veldkamp,
on account of the decision of the Doctorate Board
to be publicly defended
on Thursday 13 July 2023 at 16.45 hours

by

Sebastiaan Waanders

born on the 16th of January 1985
in Zwolle, the Netherlands

This dissertation has been approved by:

Supervisor
prof. dr. ir. B. ten Haken

Co-supervisor
dr. L. Alic

Cover design: A. Veugelers
Cover image courtesy of Panton - Ontwerpers voor de zorg
Printed by: Gildeprint
ISBN (print): 978-90-365-5692-7
ISBN (digital): 978-90-365-5693-4
DOI: 10.3990/1.9789036556934

Graduation Committee

Chair / secretary
prof. dr. J. L. Herek

Supervisor
prof. dr. ir. B. ten Haken — University of Twente - TNW, *Magnetic Detection and Imaging*

Co-supervisor
dr. L. Alic — University of Twente - TNW, *Magnetic Detection and Imaging*

Committee members
prof. dr. S. Conolly — University of California at Berkeley
prof. dr. F. Ludwig — Technische Universität Braunschweig
prof. dr. ir. N. Bosschaart — University of Twente - TNW, *Biomedical Photonic Imaging*
prof. dr. ir. L. Abelmann — University of Twente - EEMCS, *Robotics and Mechatronics*

Acknowledgments
The research described in this thesis was carried out at the Faculty of Science and Technology and the TechMed Centre (University of Twente). The work was partially supported by the framework of the *Pieken in de Delta* project *Arthur*, funded by the Dutch Ministry of Economic Affairs and the Provinces of Overijssel and Gelderland.

Contents

1 | Magnetic nanoparticle-based sensing in (bio)medical applications

Ever since Maxwell described the behavior of electromagnetic fields in his set of equations, mankind has applied this knowledge to a staggering array of applications. From the telegraph to mobile communications, from electrical generators and motors to IT and from metal detectors to MRI scanners, electromagnetism has played a huge role in our daily lives ever since.

Because of its lack of ionizing radiation, magnetic techniques have gained the attention in the medical world as safe and reliable alternatives. That include diagnosis and, with the advent of magnetic hyperthermia, even treatment of cancer. However, even though our cell phone and car are full of magnetic devices, biomedical applications have been limited to large and cumbersome installations like MRI scanners or magnetic cardiography. Diagnostic modalities relying on ionizing radiation still have unsurpassed selectivity and sensitivity. Magnetic techniques are lagging behind because of their sensitivity to environmental factors like electromagnetic noise and thermal instabilities, which limits these setups to magnetically shielded rooms and other carefully controlled environments. This thesis aims to unify the fields of surgical medicine and state-of-the-art magnetic research by applying lessens learned in the years since Maxwell and Faraday. The first clinical application we designed our setup around is the sentinel lymph node (SLN) procedure, which is often employed to effectively stage of breast cancer.

The SLN procedure, designed to determine the metastatic development of cancer, is the current standard of care for open surgery in many countries for breast cancer, head and neck cancer, and skin melanoma. Furthermore, research is under way to assess feasibility of the SLN procedure for colorectal, prostate, and non-small cell lung cancer. Currently, the procedure is most commonly facilitated by a radioactive tracer (a ^{99m}Tc albumin colloid) injected in near proximity of the primary tumor. The radioactive tracer is often complemented by a patent blue dye or ICG tracer. The hypothetical SLN are detected by the gamma probe, with a final confirmation the nodal status by the pathology afterwards. The entire lymphatic basin draining the tumor is therefore assessed under the assumption that SLN a refection is of the whole lymphatic basin. Consequently, SLN procedure averts the full axillary clearance associated with severe morbidity and complications.

Although the combined method works well, the use of the radioactive tracer has drawbacks, including a significant logistical burden on the hospital, which limits its use in third world countries and other regions without access to radioisotopes. A magnetic alternative for SLN procedure is clinically available, but it is limited by noise such as the diamagnetism of the human body, and even more importantly, the (metallic) surgical instruments which createe a constant need to balance the instrument intra-operatively. In addition, the penetration depth of such a single-coil magnetometer is limited by the diameter of the excitation coil, which is approximately 1.5-2cm. We believe that by isolating the magnetic signature of the tracers we can improve the selectivity of such a magnetometer, which will increase the penetration depth by adding a compact external excitation system that is placed beneath the patient.

Superparamagnetic iron oxide nanoparticles (SPIONs) are successfully implemented in various (bio)medical applications, such as Magnetic Particle Imaging (MPI), magnetic immunoassays, and Magnetic Resonance Imaging (MRI). However, all these applications are capital-intensive and cumbersome, limiting their use in the operating theatre due to stringent requirements with regards to, for example, background magnetic fields. Still, the unique magnetic signature of these particles opens up a world of opportunities in perioperative diagnostics, and we aim to bring such a handheld system using nanoparticles into the operating theatre.

This thesis addresses the development of a selective and sensitive handheld magnetometer for in vivo intra-operative detection of SPIO nanoparticles. Intended use of this magnetometer is SLN procedure in breast cancer, and its design reflects the specific needs for this case. However, it should be noted that this is but a single implementation of a magnetometer employing the so-called Differential Magnetometry (DiffMag) principle. In the last chapter of this thesis we will explore the potential of DiffMag in a number of different pathologies and applications.

1.1 Electromedicine in medicine

The magnetic tracers in medical applications are excessively used in radiology where various compounds are utilised for altering local magnetization for positive or negative contrast on magnetic resonance imaging (MRI). The same compounds were used off-label for magnetic SLN procedure. In ex vivo use, magnetic tracers are employed in various in vitro diagnostics procedures, where functionalized particles are used that attach specifically to certain cells or compounds.

There is a variety of devices relaying on magnetic field sensing in various form factors, designs and working principles: e.g. Hall sensors, superconducting quantum interference devices (SQUIDS), Faraday induction sensors. In its simplest form, a Faraday sensor is a simple loop of conducting wire. When placed in a time-varying magnetic field, the loop will induce a current referred to as Faraday effect. The magnitude of this induced current scales with the amplitude and frequency of the magnetic induction field, which is a sum of the surrounding magnetic field and magnetization. The other way around, driving a current through a coil of wire generates a magnetic field. The Faraday principle is perhaps the most fundamental principle underlying practical applications of magnetism

The work described in this thesis revolves around a special class of magnetic tracers called *superparamagnetic iron oxide nanoparticles* or *SPIONs*. These particles consist of an iron oxide (Fe_3O_4 or Fe_2O_3) core, encapsulated by a biocompatible coating, and potentially functionalised. Usually, we consider these particles as core-shell particles with a spherical core, but other shapes and sizes exist as well. SPIONs are an interesting particle family because of the low toxicity of the compound, and high degree of customization that is possible with tailored engineering of both the magnetic core and the (functionalized) coating.

1.2 Design application: the Sentinel Lymph Node

Contrary to typical technology-push development cycles, our research originated from an unmet clinical need. Surgeons in the local MST hospital encountered serious logistical challenges implementing the SLN procedure as current-standard-of-care for breast cancer surgeries. Currently available AC-magnetometry based solutions proved inadequate at the time, and research set out at the University of Twente to investigate improvements. This resulted in the nationally funded PIDON project *Arthur*, in which the University of Twente set out to collaborate with a consortium consisting of the companies Panton, Kryoz (now part of the Demcon group) and DKMS and the hospitals MST and Radboudumc.

1.3 Thesis outline

This thesis describes development of a small handheld probe intended for reliable SPION detection during surgery. Accordingly, we needed a technology which shares the selective character of radioactive methods whilst staying within the safety limits imposed upon the use of non-ionizing radiation. Moreover, the additional medical training for this handheld probe needed to be kept at minimum.

Chapter 2 presents the patented processing principle (DiffMag) as an alternative for AC magnetometry. This approach utilizes the unique non-linear magnetic properties of SPIONs to eliminate the drawbacks of both the traditional gamma-radiation centered approach and the drawbacks of clinically used magnetic probes. Magnetic field amplitude of DiffMag is limited to 5mT enabling handheld operation without additional cooling. The DiffMag ensures the processing sensitivity without a need for external re-balancing.

Chapter 3 describes how one of the main limitations of the current implementation of the DiffMag probe - its limited penetration depth - can be circumvented by a radical new magnetometer design. Here, we describe efforts to separate excitation and detection coils, which is made possible by the piecewise fashion in which the DiffMag excitation field sequence is constructed. This uniquely allows for dynamic compensation of the varying mutual inductance between excitation and detection coils. By separating excitation and detection coils, the excitation coils can be made much larger, increasing field penetration, whereas the spatial accuracy of detection is guaranteed by the small detection coils.

Chapter 4 focuses to the second part of the equation, the tracer material. An optimal scenario requires both a sensitive magnetometer and an optimized magnetic tracer in order to maximize the system's sensitivity without requiring substantial amounts of tracer material to be injected into the patient. Therefore, we study the magnetization dynamics of magnetic nanoparticles in the relevant low frequency and low field regime in Chapter 3. Here, we extend the familiar approach of solving the Fokker-Planck equations for both relaxation mechanisms by introducing a subtle coupling between both equations, and validate the model using commercially available magnetic tracers.

Chapter 5 includes a general discussion about Differential Magnetometry, as presented in this thesis, and provides an outlook on further technical developments and new clinical applications for this platform technology.

2 | Differential Magnetometry

Sentinel Lymph Node biopsy has become a staple tool in the diagnosis of breast cancer. By replacing the morbidity-plagued axillary node clearance with removing only those nodes most likely to contain metastases, it has greatly improved the quality of life of many breast cancer patients. However, due to the use of ionizing radiation emitted by the technetium-based tracer material, the current Sentinel Lymph Node biopsy has serious drawbacks. Most urgently, the reliance on radioisotopes limits the application of this procedure to small parts of the developed world, and it imposes restrictions on patient planning and hospital logistics. Magnetic alternatives have been tested in recent years, but all have their own drawbacks, mostly related to interference from metallic instruments and electromagnetic noise coming from the human body. In this paper, we demonstrate an alternative approach that utilizes the unique nonlinear magnetic properties of superparamagnetic iron oxide nanoparticles to eliminate the drawbacks of both the traditional gamma-radiation centered approach and the novel magnetic techniques pioneered by others. Contrary to many other nonlinear magnetic approaches however, field amplitudes are limited to 5mT, which enables handheld operation without additional cooling. We show that excellent mass sensitivity can be obtained without the need for external re-balancing of the probe to negate any influences from the human body. Additionally, we show how this approach can be used to suppress artefacts resulting from the presence of metallic instruments, which are a significant dealbreaker when using conventional magnetometry-based approaches.

This chapter was published as *A handheld SPIO-based sentinel lymph node mapping device using differential magnetometry* by S. Waanders, M. Visscher, R.R. Wildeboer, T.O.B. Oderkerk, H.J.G. Krooshoop and B. ten Haken, *Physics in Medicine & Biology* 61 (22), 8120. Additionally, the DiffMag principle outlined here was patented as *Method and apparatus for measuring an amount of superparamagnetic material in an object*, US Patent 10031106 (2018). The author of this thesis contributed to this work by describing the DiffMag physics, implementing the measurement software, designing the hardware, characterizing the system's performance and writing both manuscripts.

2.1 Introduction

The Sentinel Lymph Node (SLN) procedure is a standard tool to assess the point to which certain cancers have developed[1]. It is the current standard of care for breast cancer and melanoma in many countries[2]. Currently, the procedure is most commonly performed by injecting a combination of a blue dye and a radioactive nanocolloid (^{99m}Tc albumin) near the tumor, after which the lymphatic drainage path is followed by a gamma probe until a lymph node is found (Figure 2.1). By performing histopathology on this lymph node, the nodal status of the entire lymphatic basin draining the tumor area can be determined, potentially sparing the patient a full axillary clearance, which is associated with severe morbidity and complications[3].

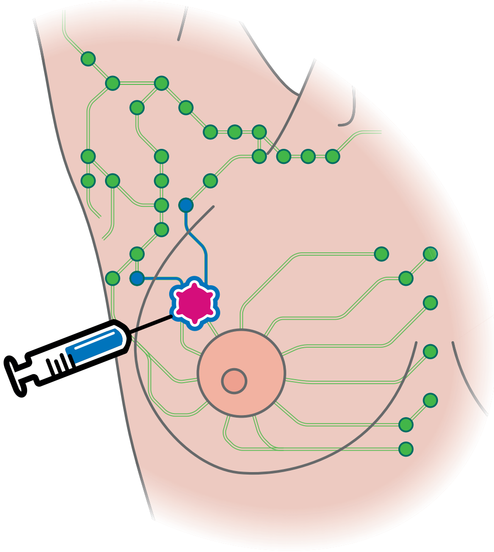

Figure 2.1: Schematic representation of the Sentinel Lymph Node localization procedure, showing the peritumoral injection site, and tracer travelling to two sentinel lymph nodes.

Although the combined method works well, the use of the radioactive tracer has drawbacks, including a significant logistical burden on the hospital, which limits its use in third world countries and other regions without ready access to radioisotopes[4]. However, a key effort is underway to develop a magnetic alternative to the previously mentioned radioactive method[5][6][7], but this approach is limited by inductively coupled noise stemming from the diamagnetism of the human body, which creates a constant need to balance the instrument intra-operatively[8]. We believe that by specifically searching for the nonlinear magnetic signature of the magnetic tracer used (for example, *Resovist™*, Bayer Schering Pharma GmbH), we can improve the selectivity and sensitivity of such a magnetometer setup and thus increase its clinical applicability. Additionally, conventional magnetometry-based techniques are hampered by the presence of metallic objects like surgical instruments, as they induce noise into the instruments, rendering them useless. Our demonstrated approach negates these noise sources, and enables effortless integration of the technique into standard clinical practice.

The use of superparamagnetic iron oxide nanoparticles (SPIONs) has been successfully implemented in various medical and biological applications[9], such as Magnetic Particle Imaging (MPI)[10], magnetic immunoassays[11][12] and Magnetic Resonance Imaging (MRI)[13]. However, all these applications are capital intensive and cumbersome, limiting their use in the operating theatre due to stringent requirements with regard to, for example, background magnetic fields. Still, the unique magnetic signature of these particles opens up a world of opportunities in diagnostics, and we aim to bring such a system using nanoparticles into the operating theatre.

This chapter describes the development of a handheld magnetic nanoparticle detector suitable for intra-operative use. It is specifically aimed at exploiting the nonlinear magnetic properties of these particles, using a measurement sequence we introduced as *Differential Magnetometry*[8], which is currently patent pending[14]. We describe the development and characteristics of the handheld device and briefly explore possible strategies for improving the system's resolution and other performance figures.

2.1.1 **Clinical requirements**

The starting point of any development process for a medical apparatus should be the clinical case at hand, and it is no different here. A few considerations must be made with regards to user friendliness of the device, considering its usage by a medical professional in the operating theatre. For proper adoption of magnetic sensing technology in the operating room, the sensor should be robust against electromagnetic noise coming from other equipment, as well as the tools used by the surgeon during the procedure. With these tools being made primarily out of surgical (carbon) steel, magnetic interference from scalpels, retractors et cetera is a serious problem for conventional alternating current (AC) magnetometry. In that approach, the generated magnetic field is strongly perturbed by these instruments, which leads to erroneous signals from the probe. Additionally, the non-constant magnetic susceptibility of the human body forms another resolution limiter. However, all these unwanted signals have in common that their magnetic behavior in the low field (mT) regime is linear.

Conventional alternating current (AC) magnetometry has proven to be an accurate tool for establishing the magnetic properties of a sample[15]. A sample is subjected to an alternating magnetic field, which results in an alternating magnetization of the sample. It is then, via Faraday's principle of induction, detected by a sensitive search coil, usually placed coaxially with the excitation coil. The resultant measurement is of the net magnetic susceptibility of the total sample volume probed by the detection coil. However, this leads to the limitations of a conventional ac magnetometer with regards to intra-operative detection.

Consider a tissue sample in which SPIO nanoparticles are placed. These particles, with a large (superpara)magnetic moment, usually dominate the measured signal for moderate amounts of SPIONs, as their magnetic susceptibility χ_0 is roughly seven orders of magnitude higher than that of the surrounding diamagnetic tissue. However, as the particle concentration reduces, so does the part of the signal originating from the nanoparticles, which at some point becomes of the same order of magnitude as the signal from the diamagnetic tissue. At this point, it becomes hard to localize the particles because of the low signal to noise ratio (SNR). This means that the maximum attainable sensitivity of such a probe is not limited by the hardware or noise performance of the probe itself, but rather by the tissue under investigation, which is a limitation that cannot be alleviated without obtaining a specific contrast between the SPIONs and the tissue sample[16].

From animal studies[17][18] performed with AC magnetometers, we know that for ferucarbotran tracers, as little as 10μ g iron (Fe) of tracer material ends up in the clinically relevant Sentinel Lymph Nodes, and that they are located up to four centimeters deep in the body. Because the nodes are found intraoperatively, this depth requirement is not as strict as that, but still we aim for a mass resolution of our system of 5μg Fe directly underneath the probe to accurately assess all localized nodes for the presence of SPIONs.

Additional requirements stem from the geometry of the surgical procedure. Many procedures nowadays are executed in the least invasive way possible, meaning that any probe which is to be inserted into the surgical cavity should be as thin as possible to minimize obstruction of the surgeon's field of view. Our probe is designed with a 20 mm outside diameter to accomodate this, similar to the outside diameter of clinically applied gamma probes.

2.2 Differential Magnetometry

Superparamagnetic iron oxide nanoparticles have been extensively studied as contrast materials in magnetic resonance imaging, and are slowly making their way into other medical applications. These particles consist of a 6-10nm sized iron oxide core, encapsulated in a coating of biocompatible material, such as (carboxy)dextran. The use of these particles in magnetic resonance imaging and standard magnetometry is based on the strong magnetic susceptibility χ when exposed to an external magnetic field. However, as explained in the previous section, as the amount of contrast agent decreases, this magnetic signature becomes obfuscated by the diamagnetic signal contribution of the surrounding tissue. To reliably detect small amounts of particles in a big volume containing other materials, one should obtain a signal which is specific to the particles, much like the radiation signature of the ^{99m}Tc albumin colloid used in the radioactive method.

This specific signature can be found in the strongly nonlinear magnetization characteristics of the SPIO nanoparticles, which contrasts with the linear magnetization curve of tissue, which is mostly diamagnetic. By exposing the sample under investigation to a sequence of varying and static magnetic fields, we specifically target the SPIO nanoparticles and are thus able to localize them in tissue.

The magnetization of a single SPIO nanoparticle is governed (in the simplest approximation) by the so-called *Langevin* equation:

$$M = M_s\mathcal{L}\left(x\right) \qquad \mathcal{L}\left(x\right) = \coth x - \frac{1}{x} \tag{2.1}$$

where x represents the dimensionless magnetic field: $x = \frac{\mu_0 mH}{k_b T}$

As can be seen in Figure 2.2, this leads to a strongly nonlinear magnetization curve, which saturates for high applied fields, where all magnetic

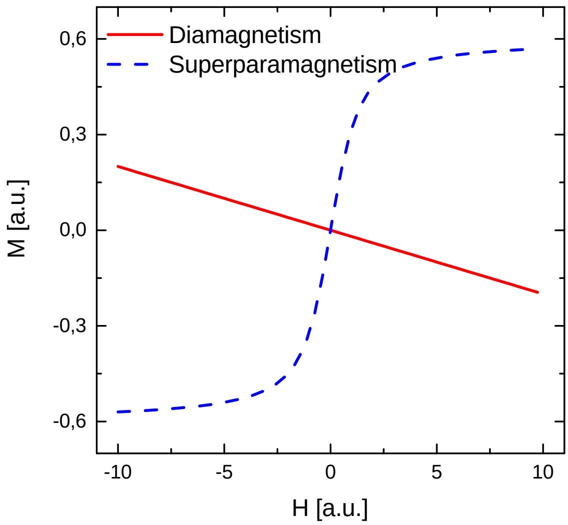

Figure 2.2: Magnetization vs applied field for an ideal SPIO nanoparticle (blue) and a diamagnetic material (red)

moments within the particle ensemble are aligned and the magnetization of the particle can no longer increase.

When a sample containing superparamagnetic iron oxide nanoparticles is exposed to a small oscillating magnetic field H_{ac}:

$$H_{ac} = S_{exc} \frac{I_{ac} \sin \omega t}{\mu_0}, \tag{2.2}$$

where S_{exc} is the coil constant of the excitation coil in [T/A], I_{ac} the excitation current and ω the oscillation frequency, this will result in an oscillating magnetization, which is picked up as a voltage over the detection coil.

This is the basis of conventional magnetometry, in which the detection voltage scales with the *derivative* of the magnetization curve around zero, or the *magnetic susceptibility* χ. However, diamagnetic contributions from the tissue surrounding the nanoparticles also contribute to this signal, and can, in principle, obscure the signal coming from a small amount of particles.

Differential Magnetometry (DiffMag) uses the nonlinearity of the magnetization curve of SPIO nanoparticles, whereas the background signal is linear, even for moderately strong fields(Figure 2.2). Interestingly, this nonlinearity is already strongly present at low fields in the order of 1mT, which allows for a low-power solution, ideal for intra-operative use with simple hardware. By applying a series of alternating offset fields with amplitude H_{dc} to the sample while probing the derivative of the magnetization curve $\frac{dM}{dH}$, we can compare the value of this derivative at various points on the curve, enabling us to distinguish between linearly magnetic tissue and superparamagnetic particles. The resulting field sequence is shown in Figure 2.3.

Mathematically, the DC excitation pulse is defined as

$$H_{dc} = h_{dc}\Gamma(t) \tag{2.3}$$

$$\text{with} \quad \Gamma(t) = \begin{cases} 1 & \tau/4 < t < \tau/2 \\ -1 & 3\tau/4 < t < \tau \\ 0 & \text{elsewhere} \end{cases} \tag{2.4}$$

Here, τ defines the duration of a single, full DiffMag cycle, and h_{dc} the amplitude of the pulse. At the detector, the detected signal amplitude u depends on the amplitude of the alternating sample magnetization M:

$$u = -2\pi f S_{det}(z) V_c M \tag{2.5}$$

where f is the excitation field frequency, $S_{det}(z)$ the coil constant (in T/A) and V_c the magnetic core volume.

The single-cycle DiffMag signal is defined as

$$\begin{aligned} \Delta\bar{u} &= \frac{1}{2}\left[\Delta\bar{u}_+ + \Delta\bar{u}_-\right] \\ &= \frac{1}{2}\left[(\bar{u}_0 - \bar{u}_+) + (\bar{u}_0 - \bar{u}_-)\right] \end{aligned} \tag{2.6}$$

Here, $\bar{u}_0$ represents the mean voltage in the absence of a pulse, and $\bar{u}_-$ and $\bar{u}_+$ represent the mean sensor voltage during a negative and positive pulse, respectively. The polarity change in the pulse allows for compensation of local field imbalances, for example due to the earth's magnetic field. Earlier, we demonstrated the efficacy of this procedure in a laboratory setting[8], allowing us to focus on a practical real-world application now. This procedure results in background-independent detection of SPIO nanoparticles, in which the measured signal scales linearly with the amount of nanoparticles, but drops off with distance, following Ampère's law.

2.2.1 **Noise compensation**

Various sources influence the voltage resulting from the detection circuit before calculating the DiffMag signal, many of which are not related to the

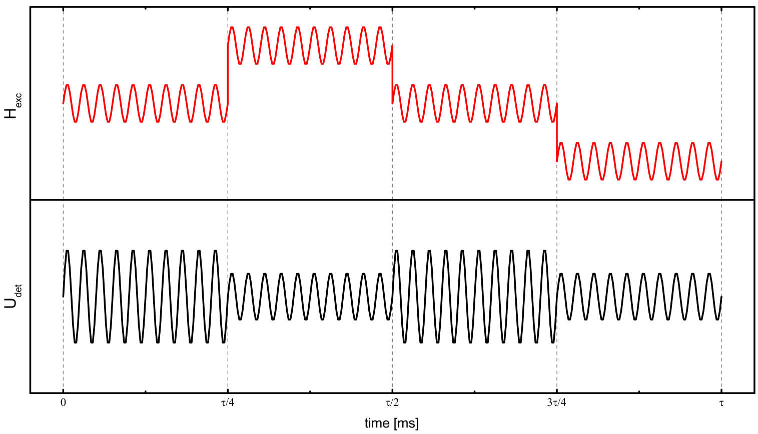

Figure 2.3: DiffMag modulated excitation field (top), resultant detector voltage (bottom). Figure not to scale.

particles used. Most of these are reliably filtered out by signal reconstruction, but the large inductive load on the coils may cause dynamic range problems, so a compensation strategy was developed to dynamically cancel out unwanted noise contributions.

The inherent differential nature of the DiffMag pulse sequence allows for subtraction of an arbitrary baseline value, as long as this baseline is kept at a constant value throughout one measurement cycle. This allows for electronic compensation of any linear magnetic or electronic influences that would otherwise cause the sensor voltage to drift outside of the dynamic range of the receive chain, which is limited to obtain excellent sensitivity. This sensor drift can be caused by a variety of phenomena, like heating and subsequent thermal expansion of the excitation coil, but also from the presence of stray magnetic fields originating from magnetized surgical tools, for example. This is implemented by means of a compensation coil wound around the detection gradiometer, which couples a small, controlled amount of magnetic flux into the detection coils to cancel any imbalances.

Mainly though, noise is suppressed by isolation of the main frequency through a process known as *synchronous detection*, where the orthogonality of sines is exploited. Using the excitation signal as a reference, the detected signal is multiplied with the reference. This yields a signal U_{psd} containing the sum and difference frequency components from signal and reference (Eq. 2.9).

$$U_{det} = u_{det} \sin(2\pi f t + \phi_{det}) \tag{2.7}$$

$$U_{ref} = \sin(2\pi f t + \phi_{ref}) \tag{2.8}$$

$$U_{psd} = \frac{1}{2} u_{det} \left[\cos(\phi_{ref} - \phi_{det}) - \cos(4\pi f t + \phi_{ref} + \phi_{det})\right] \tag{2.9}$$

In the special case where the signal frequency is equal to the reference frequency, the DC component of Equation 2.9 is a measure which scales with the desired signal intensity. This DC signal is isolated by low-pass filtering of the multiplied signal.

This allows us to recover the original measured signal, without noise:

$$u_{det} = \sqrt{X^2 + Y^2} \quad \text{and} \quad \phi_{det} = \tan^{-1}\left(\frac{Y}{X}\right) \tag{2.10}$$

$$\text{with} \quad X = u_{det} \cos(\phi_{det}) \quad \text{and} \quad Y = u_{det} \sin(\phi_{det}) \tag{2.11}$$

2.3 Experimental setup

The DiffMag handheld system is comprised of three parts: the probe itself, the base unit and a PC which performs all the signal analyses. In the following sections we describe the system in detail.

2.3.1 Probe design and implementation

To assess the feasibility of the concept introduced in the previous section, a prototype was constructed consisting of an excitation coil surrounded by a detection coil pair which generates the field sequence magnetizing the SPIO nanoparticles. To cancel out the mutual inductance between the detection coil and the excitation coils, the excitation coil pair are placed in series with their polarities reversed, acting as a gradiometer. This first-order compensation minimizes the influence of the excitation signal on the detector. The excitation coils are wound with litz wire (Rupalit HF Litze V155, 27x0,071mm +2x52) to minimize AC losses. A small compensation coil pair is wound around the detection coils to allow for dynamic field compensation and imbalance correction. All coils were wet wound in epoxy resin (Stycast 1266) to prevent wire movement due to thermal or mechanical stress. The coils are wound on a body composed of a aluminumnitride-boronnitride composite (SHAPAL™Hi-M soft, Ceratec Technical Ceramics BV, The Netherlands), mainly because of its excellent thermal conductivity and low thermal expansion coefficient. To accommodate for the high

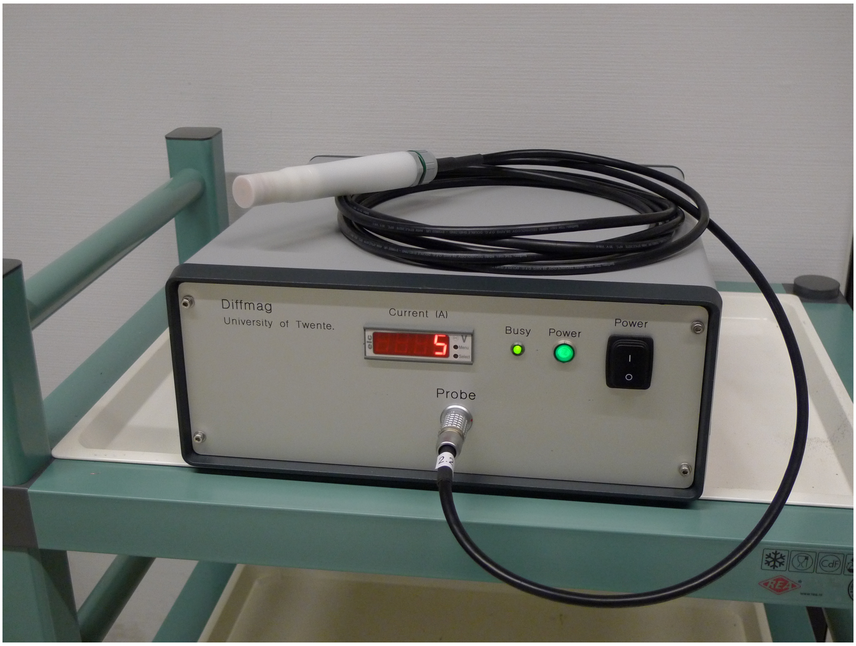

Figure 2.4: Handheld DiffMag prototype

hygiene requirements posed by the medical environment in which the probe will operate, the entire probe assembly is placed inside a delrin enclosure for easy cleaning and aesthetics. Figure 2.4 shows the assembled prototype device and its base unit.

The probe body additionally contains a first filter stage (bandpass with 3dB points at 1kHz and 15kHz) which acts as a decoupler between the connecting cable and the coil setup. The coil is driven by a purpose-built current driven amplifier (ServoWatt, 24V 2A continuous, 4A peak output), connected by a shielded cable. The excitation signal is monitored through a shunt resistor in the power amplifier and fed back into the data processing unit to serve as a reference for phase-sensitive signal processing.

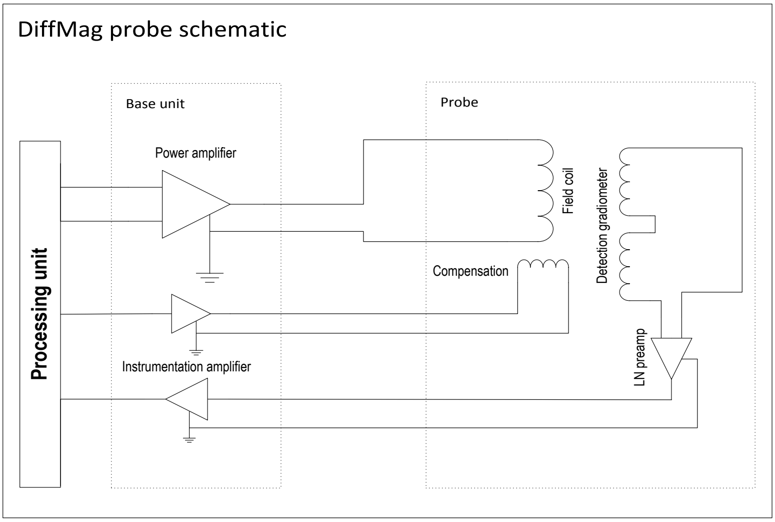

Figure 2.5: System level electronics description

Results

2.4.1 Probe characteristics

Tracer sensitivity

The main characteristics of the handheld probe are of course its attainable mass sensitivity, its penetration depth and the lateral sensitivity of the device. A higher sensitivity means that even nodes with the tiniest amounts of SPIONs can be found reliably, whereas an increased penetration depth means that it is easier to localize deeper lying nodes. Finally, a high lateral sensitivity (i.e. a spatially selective probe) is required to distinguish between multiple closely located nodes. Figure 2.6 shows the measured dose-response curve for the handheld DiffMag probe and a set of artificial lymph nodes containing varying concentrations of Resovist. Four samples were omitted due to obvious leakage of the container. Samples up to 5μgFe can reliably be detected above the noise threshold.

Spatial sensitivity

For reliable operation of the probe during surgery, the probe needs to have a high spatial sensitivity, i.e. the probe's axial full width half max (FWHM) needs to be small. The lateral sensitivity is shown in Figure 2.7. Here, we

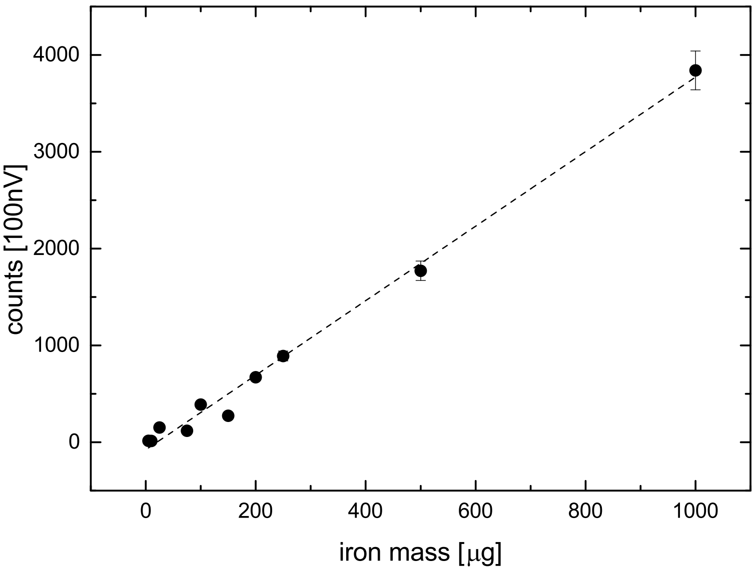

Figure 2.6: Dose-response curve for Resovist nanoparticles with the DiffMag handheld probe operated at 2.5kHz AC.

see that the FWHM is 25mm, which is strongly influenced by the fact that our phantom lymph node containing the SPIO tracer has a width of 5mm. This could be improved by decreasing the probe diameter, which comes at the cost of strongly reduced penetration depth.

Penetration depth

Furthermore, the penetration depth of the probe determines the depth at which a sample of magnetic nanoparticles can be located. Due to the fact that our probe is a simple gradiometer configuration, the penetration depth is of the order of the probe's diameter. The result of this measurement is shown in Figure 2.8. As can be seen here, a sample of 500μgFe can be measured up to 1.0cm depth. This is sufficient for intraoperative use, but it rules out the possibility of transcutaneous detection of deeply located sentinel lymph nodes prior to incision. If transcutaneous detection is required, a different sensor geometry is required. For example, one could separate excitation and detection coils, and use the dynamic compensation of DiffMag to dynamically decouple the mutual inductances between these two, which would allow for a large excitation coil to increase the probe's penetration depth.

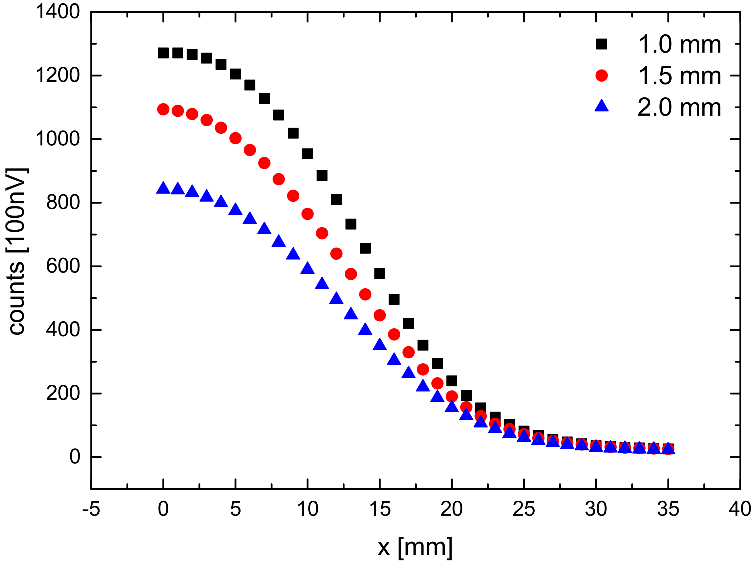

Figure 2.7: Lateral sensitivity of the DiffMag prototype for a $500\mu g$ Resovist phantom lymph node at 1.0, 1.5 and 2.0mm from probe tip.

2.4.2 Excitation optimization

The DiffMag excitation sequence gives the operator a number of parameters which influence the total signal strength obtained from a measurement for a certain type of particle. These are strongly dependent on the dynamical behavior of the particle which is used. Mainly, we are concerned with the frequency of the alternating field, f_{ac}, its amplitude (H_{ac}) and the amplitude of the pulse field (H_{dc}). It is common practice for an alternating field magnetometer to increase the driving frequency of the system, as the detector voltage scales with the frequency of the resultant alternating magnetization. However, because the dynamical behavior of the SPIO tracer depends strongly on both the Brownian and Neel relaxation constants, we find an optimum frequency of 2.5kHz. If the frequency is further increased, the particle signal decays because of lagging Brownian relaxation behavior.

Then, the two parameters that need optimization next are the alternating and offset field amplitudes. These are limited not by the physics of the particle dynamics, but rather by the heat dissipation of the probe itself. As it is a compact handheld instrument, heat production needs to be minimized, and therefore power dissipation is limited. Setting the maximum heat dissipation to 1W, we can now determine the optimal excitation pa-

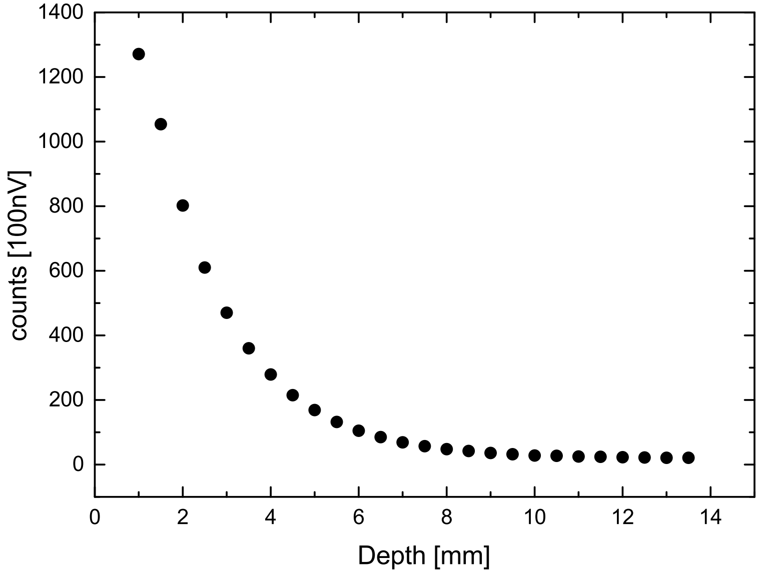

Figure 2.8: Penetration depth measurement of the DiffMag prototype, measured with a $500\mu g$Fe Resovist phantom lymph node.

rameters. As can be deduced from the magnetization curves for our tracers, the alternating magnetization scales linearly with the AC amplitude, but increasing the DC power leads to a higher signal increase because of the strong nonlinearity and the DiffMag principle. Optimal performance of the probe under constant probe temperature was achieved using an AC amplitude of $I_{ac} = 0.25A$ and and pulse amplitude of $I_{dc} = 1.5A$ using a 30% duty cycle.

Another important limiter for emitter power are the biological limits with regards to specific absorption rate (SAR) and peripheral nerve stimulation (PNS), as described in the ICNIRP guidelines[19]. We find that for these excitation parameters, we are still a factor of 10 inside these limits.

2.4.3 Noise and tissue attenuation

From a clinical point of view, the main prohibiting factor for using sensitive magnetometers during surgery is the presence of surgical instruments, made out of surgical steel, in the vicinity of the probe. The excitation field generates eddy currents inside these materials which couple a huge inductive load into the detection coils, which leads to overloading of the signal processing units, rendering the probe useless in these circumstances. The builtin dynamic compensation in the DiffMag probe detects the (linear) inductive load and generates a cancellation field through the compensation coil pair, negating the effect of the surgical steel. The result of this can be seen in Figure 2.9. Here, we see the signal from a 200μg Fe Resovist sample next to that of a human hand and surgical steel retractor instrument held next to the sample. We operate the probe in both AC magnetometry and DiffMag mode at constant AC amplitude and frequency, and compare the results. In AC mode, we measure a huge signal from the retractor, which completely obfuscates the SPIO signal. When operating in DiffMag mode, the signal from the retractor is significantly reduced, and the SPIO sample clearly stands out. Also noticeable is the slightly negative signal from the human hand in AC mode, and the strong attenuation of this diamagnetic signal in DiffMag mode.

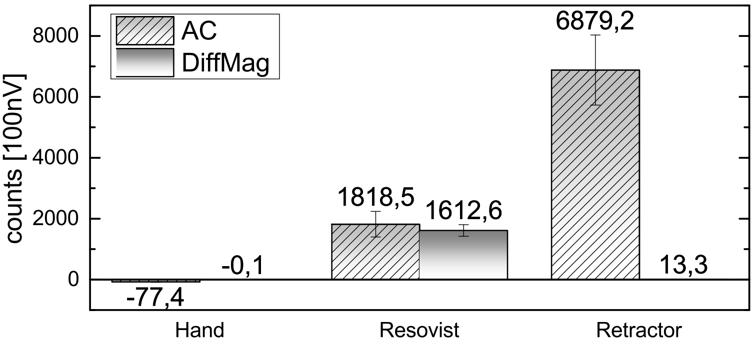

Figure 2.9: Signal counts for a 200μg Fe Resovist tracer, a human hand and a surgical steel retractor, in AC mode (left) and DiffMag mode (right).

An additional cause of problems in conventional magnetometers is signal drift due to thermal stress. The heat dissipation of the excitation coil causes a change in the mutual induction between the coils because of thermal expansion, which leads to an increasing imbalance of the gradiometer. This results in a drifting output voltage. Because of the differential nature of DiffMag, and the fact that the timescale of a single DiffMag sequence (40ms) is much shorter than the timescale at which thermal drift occurs, we have not observed any drift of the output signal in DiffMag mode.

Because of the excellent attenuation of external noise, both inductive and resistive, the noise floor of the device is composed of different noise sources inside the electronics of the probe itself. The main cause of noise is thermal or Johnson noise in the resistive components of the setup and the power amplifier and the quality of the data acquisition system. The total noise figure of the sensor was measured to be $12nV/\sqrt{Hz}$.

2.5 Discussion

In this paper, we have shown that selective detection of magnetic nanoparticles in a diamagnetic environment is feasible, and can be implemented in a compact, low power, handheld device. However, some points for improvement are still standing, mostly related to the penetration depth of the probe (i.e. the depth at which SPIO-positive nodes can be detected), and the dynamic compensation. Here, we address both points and compare the demonstrated approach to currently employed techniques.

2.5.1 Penetration depth

From literature it is known that in the case of breast cancer, sentinel lymph nodes are found at an average depth from the skin of 4.5cm. Combined with the lowest concentration of SPIONs observed in trials (10 μg Fe), this leads to a stringent resolution requirement, which is currently unmatched by both conventional magnetometry and differential magnetometry. This low penetration depth is primarily governed by the small probe diameter, which dominates the field penetration in Ampère's Law. In an earlier article, we have shown that for a conventional magnetometer, simply increasing the probe diameter does not actually increase sensing depth, as the amount of tissue probed increases as well. For DiffMag, this limitation is nonexistent, and therefore increasing the probe diameter offers a straightforward approach to measuring the presence of SPIO-positive lymph nodes transcutaneously. This can be done by adding a second, larger probe to the setup to measure the transcutaneous hotspot, and using the smaller diameter probe intra-operatively.

2.5.2 Compensation speed

Currently, the demonstrated artefact suppression relies on fast processing of the induced signal and compensating the inductive effect of metallic artefacts close to the probe by coupling additional flux into the detection coils. The quality of this compensation method is limited by the speed at which dynamically changing effects can be compensated, which is limited due to the slow processing speed of the software. By moving signal processing to a dedicated DSP, dynamic compensation of these distorting effects can be achieved.

2.5.3 Comparison to existing techniques

When observing the entire field of sentinel lymph node biopsy, we can now distinguish four different techniques currently available to the surgeon. First is the use of blue dye as tracer material, which offers visual localization of the node, but does not allow for quantitative evaluation of nodal status. Yet, it is employed in hospitals where the use of radio-isotopes is impossible, due to inavailability of the tracer or other logistical difficulties. Second, the combined approach which uses blue dye in combination with a technetium nanocolloid. Whilst this method is proven to be very effective and reliable, its reliance on radio-isotopes limits its applicability, especially in areas of the world without access to nuclear medicine. Third, the conventional magnetometry approach has been tested in various Phase 2 clinical trials, with good results. However, its lack of selective measurements and limited penetration depth, without the possibility of significant improvements in the future, lead us to believe that the fourth approach using DiffMag is more viable and will lead to more reliable results, without relying on ionizing radiation and plastic tools. An important point to consider is the tendency towards lower applied doses of contrast agent, which requires higher probe sensitivities. This might have significant advantages in both reduction of MRI artefacts and potential toxicity effects. Clinical evaluation of this instrument is vital to assess its usability, reliability and accuracy in practice.

2.6 Conclusions

Magnetic sentinel lymph node biopsy is an excellent alternative to conventional radioisotope-based localization methods. Yet it suffers from depth and mass resolution limitations because of the linear magnetization interference from the human body surrounding the SPIO nanoparticles. In this paper, we have shown that Differential Magnetometry is a feasible alternative to conventional AC magnetometry methods, at much lower field strengths and power requirements compared to alternative (imaging) technologies. It combines the excellent spatial sensitivity of a handheld search coil with the specificity offered by nonlinear magnetization measurements used by for example Magnetic Particle Imaging and frequency mixing based immunoassays, while keeping energy requirements to a minimum. The latter advantage is a strong plus for working outside shielded rooms and in the operating theatre. We have shown linearity with regards to the amount of tracer present in the nodes, with a detection sensitivity of $5 \mu g Fe$ and sufficient depth resolution for intra-operative use. Additionally, we show good attenuation of noise caused by the presence of metallic objects close to the probe, by virtue of the relative nature of the DiffMag measurement, which allows us to dynamically compensate for these signals.

Finally, we note that by implementing this selective measure of nanoparticles without background signals from tissue or instrumentarium, this procedure removes the fundamental sensitivity limit that hampers performance of conventional magnetometers in these difficult environments. This also allows for reduction of applied tracer doses with all associated benefits. Clinical evaluation of the probe, preferrably combined with a second, large diameter probe for transcutaneous hotspot measurements is vital to move forward.

2.7 Acknowledgments

The authors would like to thank A. de Boer, B. Vroling, M. Koenrades for their contributions to development and testing of the magnetometer and J.J. Klaase, J. Futterer, R. Stemerdink, C. Joosten and P. Meutstege for useful discussions with regards to the usability and requirements for clinical implementation of the handheld magnetometer. Furthermore, the authors thank A. Veugelers for creating Figure 2.1.

Bibliography

[1] Umberto Veronesi, Giovanni Paganelli, Viviana Galimberti, Giuseppe Viale, Stefano Zurrida, Marilia Bedoni, Alberto Costa, Concetta De Cicco, James G. Geraghty, Alberto Luini, Virgilio Sacchini, and Paolo Veronesi. Sentinel-node biopsy to avoid axillary dissection in breast cancer with clinically negative lymph-nodes. *Lancet*, 349(9069):1864–1867, jun 1996.

[2] Heimen Schraffordt Koops, M. H E Doting, Jakob D. Vries, A. T M G Tiebosch, John Th Plukker, Harold J. Hoekstra, and D. Albert Piers. Sentinel node biopsy as a surgical staging method for solid cancers. *Radiotherapy and Oncology*, 51(1):1–7, 1999.

[3] Gary H. Lyman, Sarah Temin, Stephen B. Edge, Lisa A. Newman, Roderick R. Turner, Donald L. Weaver, Al B. Benson, Linda D. Bosserman, Harold J. Burstein, Hiram Cody, James Hayman, Cheryl L. Perkins, Donald A. Podoloff, and Armando E. Giuliano. Sentinel lymph node biopsy for patients with early-stage breast cancer: American Society of Clinical Oncology clinical practice guideline update. *Journal of Clinical Oncology*, 32(13):1365–1383, 2014.

[4] Muneer Ahmed, Arnie D. Purushotham, and Michael Douek. Novel techniques for sentinel lymph node biopsy in breast cancer: A systematic review. *The Lancet Oncology*, 15(8):e351–e362, 2014.

[5] Michael Douek, Joost Klaase, Ian Monypenny, Ashutosh Kothari, Katalin Zechmeister, Douglas Brown, Lynda Wyld, Philip Drew, Hans Garmo, Olorunsola Agbaje, Quentin Pankhurst, Bauke Anninga, Maarten Grootendorst, Bennie Ten Haken, Margaret A Hall-Craggs, Arnie Purushotham, and Sarah Pinder. Sentinel node biopsy using a magnetic tracer versus standard technique: the SentiMAG Multicentre Trial. *Annals of surgical oncology*, 21(4):1237–45, apr 2014.

[6] Marc Thill, Andrzej Kurylcio, Rebekka Welter, Viviana van Haasteren, Britta Grosse, Gilles Berclaz, Wojciech Polkowski, and Nik Hauser. The Central-European SentiMag study: Sentinel lymph node biopsy with superparamagnetic iron oxide (SPIO) vs. radioisotope. *Breast*, 23(2):175–179, apr 2014.

[7] A Piñero-Madrona, J A Torró-Richart, J M de León-Carrillo, G de Castro-Parga, J Navarro-Cecilia, F Domínguez-Cunchillos, J M Román-Santamaría, C Fuster-Diana, and R Pardo-García. Superparamagnetic iron oxide as a tracer for sentinel node biopsy in breast cancer: A comparative non-inferiority study. *European journal of surgical oncology : the journal of the European Society of Surgical Oncology and the British Association of Surgical Oncology*, 41(8):991–997, may 2015.

[8] M. Visscher, S. Waanders, H.J.G. Krooshoop, and B. ten Haken. Selective detection of magnetic nanoparticles in biomedical applications using differential magnetometry. *Journal of Magnetism and Magnetic Materials*, 365:31–39, sep 2014.

[9] Kannan M. Krishnan. Biomedical nanomagnetics: A spin through possibilities in imaging, diagnostics, and therapy. *IEEE Transactions on Magnetics*, 46(7):2523–2558, jul 2010.

[10] Bernhard Gleich and Jürgen Weizenecker. Tomographic imaging using the nonlinear response of magnetic particles. *Nature*, 435(7046):1214–1217, jun 2005.

[11] Hans Joachim Krause, Norbert Wolters, Yi Zhang, Andreas Offenh??usser, Peter Miethe, Martin H F Meyer, Markus Hartmann, and Michael Keusgen. Magnetic particle detection by frequency mixing for immunoassay applications. *Journal of Magnetism and Magnetic Materials*, 311(1 SPEC. ISS.):436–444, apr 2007.

[12] M. P. Nikitin, M. Torno, H. Chen, A. Rosengart, and P. I. Nikitin. Quantitative real-time in vivo detection of magnetic nanoparticles by their nonlinear magnetization. *Journal of Applied Physics*, 103(7):07A304, 2008.

[13] QA A Pankhurst, J Connolly, S K Jones, and J Dobson. Applications of magnetic nanoparticles in biomedicine. *Journal of Physics D: Applied Physics*, 36(13):167–181, jul 2003.

[14] S. Waanders, M. Visscher, T.O.B. Oderkerk, H.J.G. Krooshoop, and B. ten Haken. Method and apparatus for measuring an amount of superparamagnetic material in an object, 2012.

[15] B. W M Kuipers, I. A. Bakelaar, M. Klokkenburg, and B. H. Erń. Complex magnetic susceptibility setup for spectroscopy in the extremely low-frequency range. *Review of Scientific Instruments*, 79(1), 2008.

[16] Martijn Visscher, Sebastiaan Waanders, Joost Pouw, and Bennie Ten Haken. Depth limitations for in vivo magnetic nanoparticle detection with a compact handheld device. *Journal of Magnetism and Magnetic Materials*, 380:246–250, 2015.

[17] B. Anninga, M. Ahmed, J. J. Pouw, R. M. Fratila, B. Ten Haken, D. Westbroek, S. E. Pinder, and M. Douek. Lymphatic mapping and sentinel lymph node biopsy in an in-vivo porcine model using a novel magnetic technique. *European Journal of Cancer*, 49:S263–S263, sep 2013.

[18] Joost J. Pouw, Muneer Ahmed, Bauke Anninga, Kimberley Schuurman, Sarah E. Pinder, Mieke Van Hemelrijck, Quentin A. Pankhurst, Michael Douek, and Bennie ten Haken. Comparison of three magnetic nanoparticle tracers for sentinel lymph node biopsy in an in vivo porcine model. *International Journal of Nanomedicine*, 10:1235–1243, jan 2015.

[19] G Ziegelberger. Statement on the" Guidelines for Limiting Exposure To Time-Varying Electric, Magnetic, and Electromagnetic Fields (Up To. *ICNIRP Health physics*, 97(3):257–8, sep 2009.

3 | Separation of excitation and detection coils for *in vivo* detection of superparamagnetic iron oxide nanoparticles

A novel probe for laparoscopic *in vivo* detection of superparamagnetic iron oxide nanoparticles (SPIONs) has been developed. The main application for *in vivo* detection of SPIONs our research group aims at is sentinel node biopsy. This is a method to determine if a tumor has spread through the body, which helps to improve cancer patient care. The method we use to selectively detect SPIONs is Differential Magnetometry (DiffMag). DiffMag makes use of small magnetic field strengths in the mT range. For DiffMag, a handheld probe is used that contains excitation and detection coils. However, depth sensitivity of a handheld probe is restricted by the diameter of the coils. Therefore, excitation and detection coils are separated in our novel probe. As a result, excitation coils can be made large and placed underneath a patient to generate a sufficiently large volume for the excitation field. Detection coils are made small enough to be used in laparoscopic surgery. The main challenge of this setup is movement of detection coils with respect to excitation coils. Consequently, the detector signal is obscured by the excitation field, making it impossible to measure the tiny magnetic signature from SPIONs. To measure SPIONs, active compensation is used, which is a way to cancel the excitation field seen by the detection coils. SPIONs were measured in various amounts and at various distances from the excitation coils. Furthermore, SPIONs were measured in proximity to a surgical steel retractor, and 3L water. It is shown that small amounts of SPIONs (down to 25 μg Fe) can be measured, and SPIONs can be measured up to 20 cm from the top of the excitation coil. Also, surgical steel, and diamagnetism of water – and thus of tissue – have minor influence on DiffMag measurements. In conclusion, these results make this novel probe geometry combined with DiffMag promising for laparoscopic sentinel node biopsy.

This work was published as *Separation of excitation and detection coils for in vivo detection of superparamagnetic iron oxide nanoparticles*, by M.M. Horstman - van de Loosdrecht, S. Waanders, H.J.G. Krooshoop and B. ten Haken, *Journal of magnetism*

and magnetic materials 475 563-569 (2019). The author of this thesis contributed to this work by designing the split coil geometry, the compensation mechanics and initial design of the probe, electronics and measurement software.

3.1 Introduction

Sentinel node biopsy (SNB) is a procedure to determine the lymph node status of cancer patients [1]. As a result, it can be determined if the tumor has spread through the body and consequently patient care will be improved. In this paper, a novel probe for laparoscopic SNB is presented, as shown in Figure 3.1. Using such a minimally invasive approach results in improved short-term outcome for infections, hospital stay and quality of life compared to open surgery [2]. Laparoscopic SNB can be applied for many types of tumors, including prostate [3], bladder [4], esophageal [5] and gynecologic [6] cancers.

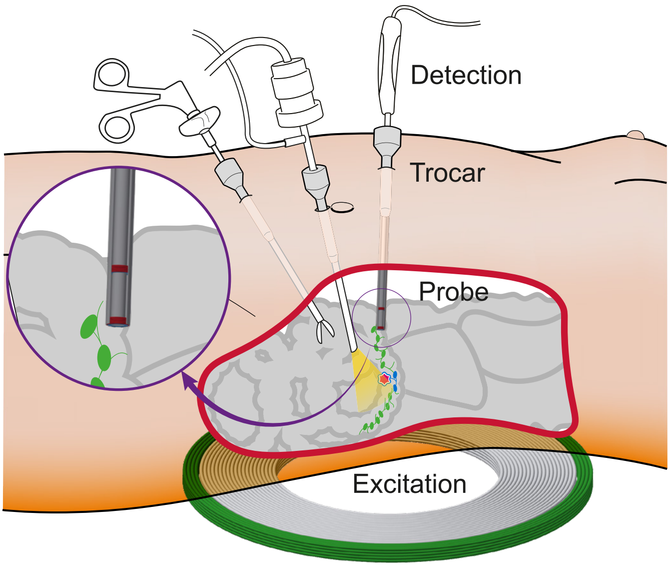

Figure 3.1: Separation of excitation and detection coils for laparoscopic sentinel node biopsies. Primary tumor is shown in pink, lymph nodes are shown in green, and sentinel nodes are shown in blue.

During SNB, a tracer is injected close to the tumor. This tracer will follow the natural path through the lymphatic system via passive mechanical transport and it will accumulate in the first nodes it encounters, namely the sentinel nodes. The next step in SNB is identification of the sentinel nodes using a dedicated probe. Finally, both the primary tumor and sentinel nodes are surgically removed.

Various types of tracers can be used for SNB. Traditionally, a radioisotope tracer is used in combination with blue dye. However, this has several disadvantages, including logistical difficulties [3]. A promising alternative is a fluorescent tracer, which is frequently used in laparoscopic surgery [7, 8]. The most important advantages of this tracer are that it can be visualized using a standard laparoscopic camera and it is possible to map lymphatic drainage pathways in real time. However, the main disadvantages are its limited depth sensitivity (<10 mm) and rapid distribution (fluorescent tracer does not get trapped in sentinel nodes), giving the surgeon limited time to find sentinel nodes [3, 7, 9].

Another promising tracer for SNB are superparamagnetic iron oxide nanoparticles (SPIONs). This magnetic tracer has many advantages over a radioactive one, since it has a long shelf life and no strict regulations [10]. The main advantage of a magnetic tracer over a fluorescent one is that SPIONs get trapped inside sentinel nodes, giving the surgeon more time to find them. Furthermore, we expect that eventually depth sensitivity will be improved with our novel laparoscopic probe.

Sentinel nodes have a mean depth of 4 cm (1.5 – 8.5 cm) in breast cancer patients [11]. Approximately 0.3% of the injection amount of SPIONs ends up in sentinel nodes [12, 13]. With a standard injection dose, it was found that a sentinel node contains 140 $\pm$ 80 μg Fe [12].

To detect SPIONs *in vivo*, several handheld probes were developed for open surgery. These probes make use of AC magnetometry [14], magnetic tunnelling junction [15], a combination of a permanent magnet and Hall sensor [12], or a fundamental mode orthogonal fluxgate gradiometer [16]. However, the main disadvantage all these probes share is their sensitivity to both surgical steel and diamagnetism of tissue. This sensitivity to diamagnetism limits depth sensitivity for low dose detection [17].

Differential Magnetometry (DiffMag) does not suffer from this disadvantage. DiffMag is a method that makes use of the nonlinear magnetic properties of SPIONs, which enables selective detection [18]. To detect SPIONs *in vivo*, a handheld probe was developed, which contains excitation and detection coils [19]. However, this first handheld probe has limited depth sensitivity. Depth sensitivity depends on the diameter of the coils. In laparoscopic surgery, the diameter of the probe is limited, because the probe has to fit through a standard laparoscopic trocar (12 mm). If the diameter of the handheld probe is decreased to 12 mm, depth sensitivity will decrease. As a result, it will be impossible to detect sentinel nodes that lie deeper in tissue, which is a prerequisite for SNB.

Our solution to improve depth sensitivity is mechanical separation of excitation and detection coils. In this way, the excitation coils can be made large to generate a sufficiently large volume for the excitation field. These large coils will be placed underneath the patient. The detection coils will be made small enough to fit through standard laparoscopic trocars and will be used as handheld probe.

The main challenge after separating excitation and detection coils is movement of the detection coils with respect to the excitation coils. As a result, the detection signal will be obscured by the excitation field and it becomes impossible to detect tiny magnetization of SPIONs. To solve this problem we make use of active compensation. In active compensation, extra field is coupled in to cancel the measured excitation field. This leads to a balanced probe and SPIONs can be measured. A second goal of active compensation is to cancel the contribution of materials with a linear magnetic susceptibility in the mT field range, such as tissue and surgical steel.

Active compensation is only possible because we use DiffMag. In DiffMag, a combination of an AC field and DC offsets is used. When a DC offset is applied, the amplitude of the measured signal is lower compared to when no offset is applied due to nonlinearity of SPIONs. The difference in amplitude between blocks with and without DC offset is defined as DiffMag counts. This is a selective, quantitative measure for SPIONs. By coupling in extra field, as is done in active compensation, the amplitude of the measured signal will change, but the difference in amplitude remains the same. Therefore, distortions in balance of the probe do not influence DiffMag measurements.

However, in conventional AC magnetometry only an AC excitation field is used. In this case, the amplitude of the measured signal is indicative for the amount of SPIONs in proximity to the probe. As a result, the extra coupled field has exactly the same effect as measuring a lower quantity SPIONs, or measuring them further away from the probe. Therefore, it is impossible to distinguish the magnetization of SPIONs from distortions in balance of the probe.

The main reason to balance the probe with active compensation is to optimize amplification gain and stay in the sensitive region of the data acquisition system. The goal of this paper is to describe and demonstrate active compensation. Furthermore, the first static SPION measurements using our novel probe are shown. Finally, it is shown that measurements are not disturbed by surgical steel or diamagnetism of tissue.

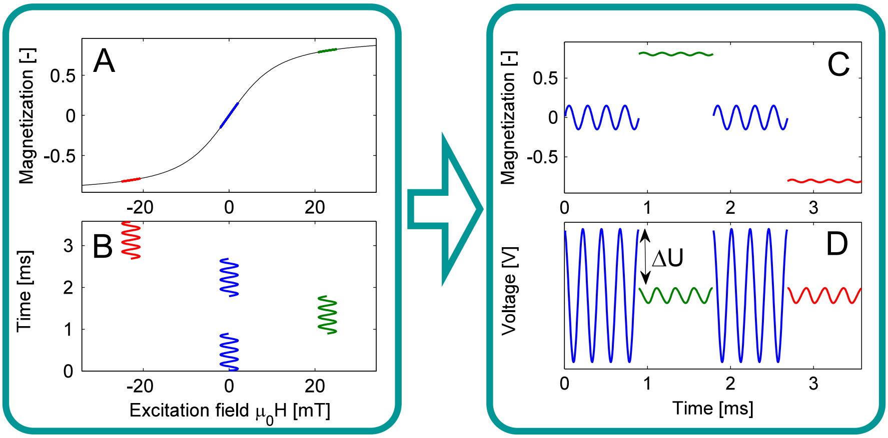

Figure 3.2: The concept of differential magnetometry simulated for monodisperse iron oxide particles with 16 nm diameter (A). The alternating excitation field is applied with intervals with a positive and negative offset field amplitude (B). The colors in each panel correspond with the offset field amplitude. Nonlinear magnetic susceptibility results in a reduced alternating magnetization response during periods with offset field (C), which is proportional to the amplitude of inductively measured signal (D). The Diffmag voltage δU specifically represents the contribution from magnetic nanoparticles in a sample. This figure is reproduced from [18]

3.2 Materials

In this paper, SHP-25 (Ocean Nanotech) particles were used. These are water soluble iron oxide nanoparticles. They have a single magnetite core with a diameter of 25 nm and a 4 nm thick amphiphilic polymer coating [20, 21]. They were measured in their standard concentration of 5 mg(Fe)/mL.

This magnetite core – polymer shell structure is typical for SPIONs. A clinical tracer is for example Sienna+®, a CE-marked magnetic tracer intended for sentinel node biopsy. This tracer also has a core-shell structure [14, 22]. However, magnetic behavior of a monodisperse particle like SHP-25 is easier to predict, so we use this particle for developmental purposes.

3.3

Methods

3.3.1 Differential Magnetometry

DiffMag is a method to selectively detect SPIONs *in vivo*, as previously described by Visscher et al. and Waanders et al. [18, 19]. It combines a continuous alternating (AC) magnetic field that has a small amplitude with positive and negative DC offset fields, as shown in Figure 3.2. As a result, every iteration of the excitation sequence consists of four blocks: no offset, positive offset, no offset, negative offset. Due to nonlinearity of SPIONs, the amplitude of the signal in a block with DC offset is lower compared to the signal in a block without DC offset. The difference in amplitude between these blocks is defined as DiffMag counts. This is a quantitative, selective measure for SPIONs.

3.3.2 Active compensation

Since the detection coils can move with respect to the excitation coils, their mutual inductance changes. As a result, the detection signal is obscured by the excitation field, making it impossible to detect tiny magnetization of SPIONs. Part of the excitation field is eliminated, because the detection coils are in a gradiometer configuration. However, to further optimize balance of the moving probe, active compensation is required. To achieve this, compensation coils are used, which are wound directly around the two detection coils. The phase and amplitude of the current that is sent through the compensation coils (and thus the magnetic field they produce) can be adjusted using two 10-bit digital potentiometers.

The induction voltage in the detection coils (U_{det}) is proportional to the time derivative of four contributions, as shown in the following equation:

$$U_{det} \propto \frac{dM_{SPION}}{dt} + \frac{dM_{lin}}{dt} + \frac{dH_{exc}}{dt} + \frac{dH_{comp}}{dt} \qquad (3.1)$$

In this equation M_{SPION} is the nonlinear magnetization of SPIONs, M_{lin} is the magnetization of materials with a linear susceptibility (for example, tissue and surgical steel), H_{exc} is the excitation field strength and H_{comp} is the compensation field strength. The goal of active compensation is to make H_{comp} equal to $M_{lin} + H_{exc}$.

The first step in active compensation is a calibration measurement. This has to be performed only once for a certain set of excitation parameters (frequency and amplitude of the AC field) for a certain probe. The detection coil signal is measured for every setting of both digital potentiometers. Next, the amplitude and phase of this signal are determined using a digital phase sensitive detection (PSD) algorithm. By fitting these results, parameters (a_0, a_1, b_0 and b_1) in the following equations can be determined:

$$R_c = a_0 + a_1 CA, \quad P_c = b_0 + b_1 CP \tag{3.2}$$

in which R_c is the amplitude, P_c is the phase, CA is the amplitude potentiometer setting (0...1023), and CP is the phase potentiometer setting (0...1023). Potentiometer settings for a desired compensation signal are given by:

$$CA = \frac{R_c - a_0}{a_1}, \quad CP = \frac{P_c - b_0}{b_1} \tag{3.3}$$

After calibration, the excitation field is turned on and the detector signal is measured. After applying the PSD algorithm, the detector signal is given by X_p and Y_p. The phase and amplitude of the current compensation signal (R_c and P_c) are know from equation 3.2, since CA and CP are known. X_c and Y_c can be calculated:

$$X_c = R_c cos(P_c), \quad Y_c = R_c sin(P_c) \tag{3.4}$$

Now, we can calculate the new compensation signal:

$$X_n = X_p - X_c, \quad Y_n = Y_p - Y_c \tag{3.5}$$

$$R_n = \sqrt{X_n^2 + Y_n^2}, \quad P_n = \tan^{-1}\frac{Y_n}{X_n} \tag{3.6}$$

Equation 3.3 will be used to determine the new potentiometer settings:

$$CA = f(R_n), \quad CP = f(P_n - \pi) \tag{3.7}$$

These settings are used in the next iteration of the DiffMag sequence.

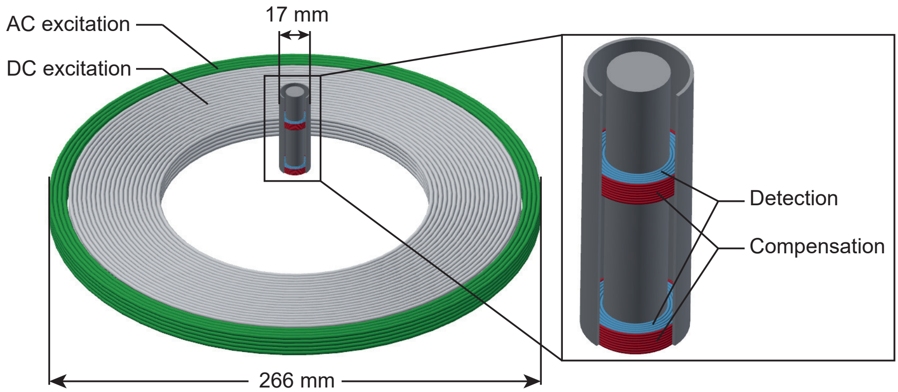

Figure 3.3: Schematic representation of coils.

	Wire ⌀[mm]	Inner ⌀[mm]	Outer ⌀[mm]	Turns [#]
DC excitation coil	2.5	146	248	100
AC excitation coil	2.5	252	266	20
Upper detection coil	0.115	10	15.5	720
Lower detection coil	0.115	10	15.5	-720
Upper compensation coil	0.115	15.5	16	40
Lower compensation coil	0.115	15.5	16	-36

Table 3.1: Specifications of the coils.

3.3.3 Experimental setup

Device

The most important part of the device are the coils, which are shown in Figure 3.3. Specifications of all coils are shown in Table 1. There are two excitations coils, one for the DC and one for the AC field. For both Litz wire is used. A transformer is connected in series to the excitation coils, but wound in opposite direction. This transformer has exactly the same mutual inductance as the excitation coils, so coupling between the coils is canceled (since the AC field would otherwise induce a current in the DC coil). Furthermore, there are two detection coils, which are in gradiometer configuration. The distance between these coils is 30 mm. Around both detection coils, compensation coils are wound.

To apply a magnetic field, a current is sent through the excitation coils. This current is provided by two power amplifiers; one for the DC coil (Servowatt DCP 390/60 50V/8A) and one for the AC coil (Servowatt

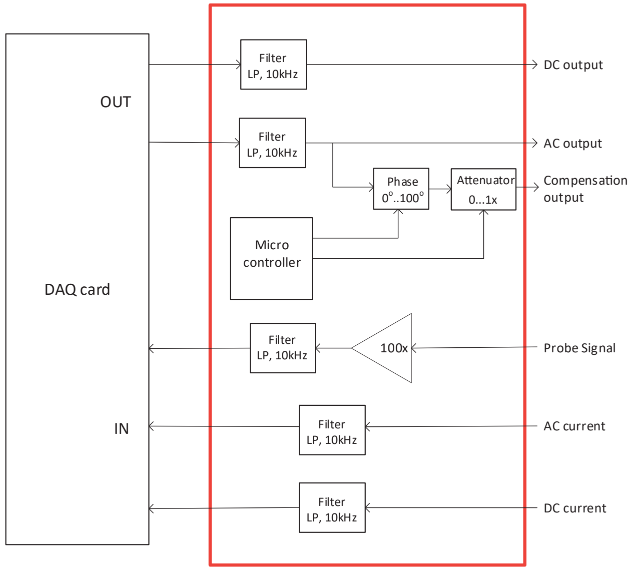

Figure 3.4: Schematic representation of signal filtering and amplification. All components in the red rectangle are present in a customized electronics box.

VM200/48A 48V/4A). The magnetic field is verified by measuring the current that is provided by the power amplifiers. These power amplifiers are controlled by a data acquisition (DAQ) card (NI USB-6356) that is connected to a PC. All input and output signals from the DAQ card are filtered (and amplified) in a customized box with electronics to prevent aliasing. The content of this box is shown in the red rectangle in Figure 3.4. The electronics box also contains two digital potentiometers to control the current sent through the compensation coils. Settings of the potentiometers are controlled by a microprocessor, which is mounted on an Arduino Uno. The signal measured by the detection coils is amplified, filtered and sent to the PC via the DAQ card. MATLAB is used both to control the system and process data.

Measurement protocol

All measurements were performed in a static setup. First, active compensation was performed, by iterating the process explained in section 3.3.2 ten times to achieve balance. In all measurements, an excitation frequency of 2525 Hz and a sample frequency of 200 kHz were used. The length of one

DiffMag sequence was set to 0.5 seconds and 20 iterations were measured. All measurements were performed three times. Three sets of measurements were performed.

First, various amounts (25, 50, 75, 100, 250 and 500 μg Fe) of SHP-25 were measured. The samples were placed directly in front of the detection coils and the detection coils were at a distance of 5 cm from the excitation coils. The currents sent were 2.4 Ampere AC and 8 Ampere DC and maximum magnetic field strengths at the location of the sample were 0.5 mT AC and 50 mT DC.

Second, the SHP-25 sample containing 500 μg Fe was measured at various distances to the excitation coils. The probe was placed at the center of the excitation coil, 1 cm above the top of the excitation coils. The sample was placed directly in front of the probe. Next, the probe and sample were moved in a straight line upwards in steps of 1 cm to a total distance of 20 cm from the excitation coils.

Last, the SHP-25 sample containing 500 μg Fe was measured in air and in proximity to a surgical steel retractor and water, in three separate measurements. The samples were placed directly in front of the detection coils and the detection coils were at a distance of 5 cm from the excitation coils. The retractor was placed directly on top of the excitation coils, between excitation coils and sample. Next, a square container containing 3L water was placed on top of the excitation coils, resulting in $\pm$ 4 cm water between excitation coils and sample.

3.4 Results

3.4.1 Active compensation

Figure 3.5 shows calibration results. The amplitude and phase of the signal from the detection coils is shown for every setting of the potentiometers.

Figure 3.6 shows ten iterations of active compensation. At the start, the excitation field is disturbing the signal, but it is gradually canceled out. After ten iterations, the probe is balanced and SPIONs can be measured.

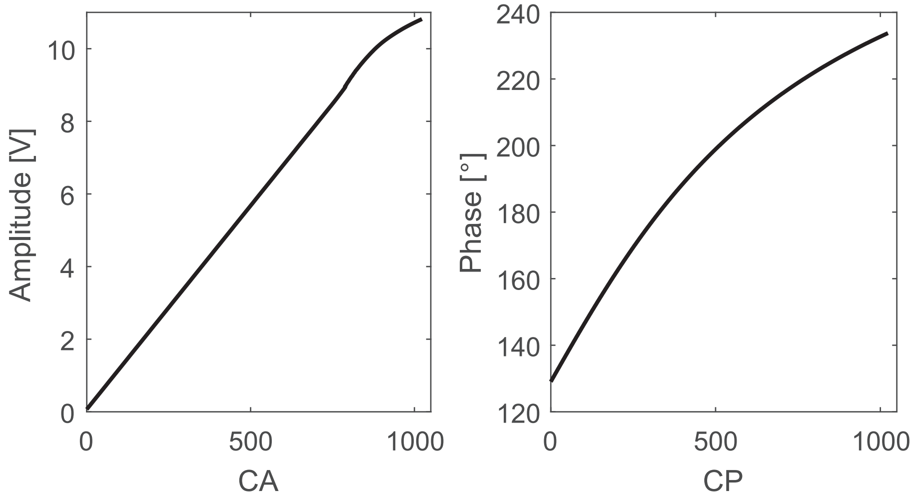

Figure 3.5: Calibration results showing amplitude and phase of the signal from the detection coils for every setting of the potentiometers. At the highest values of CA the amplitude bends, because the DAQ card has a range of ± 10 V.

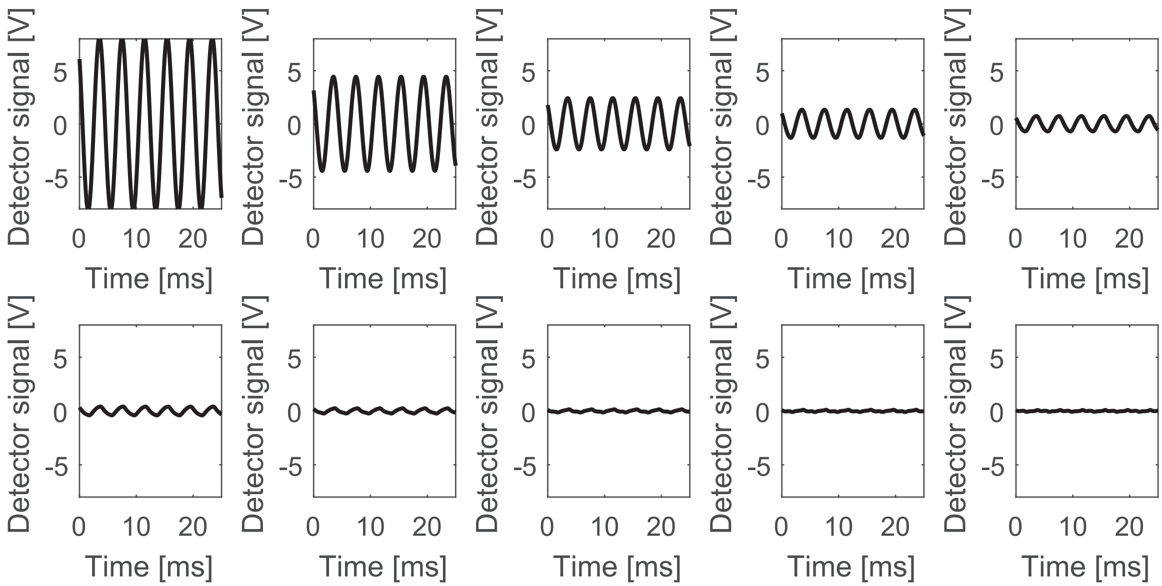

Figure 3.6: Ten iterations of active compensation, after which the probe is balanced.

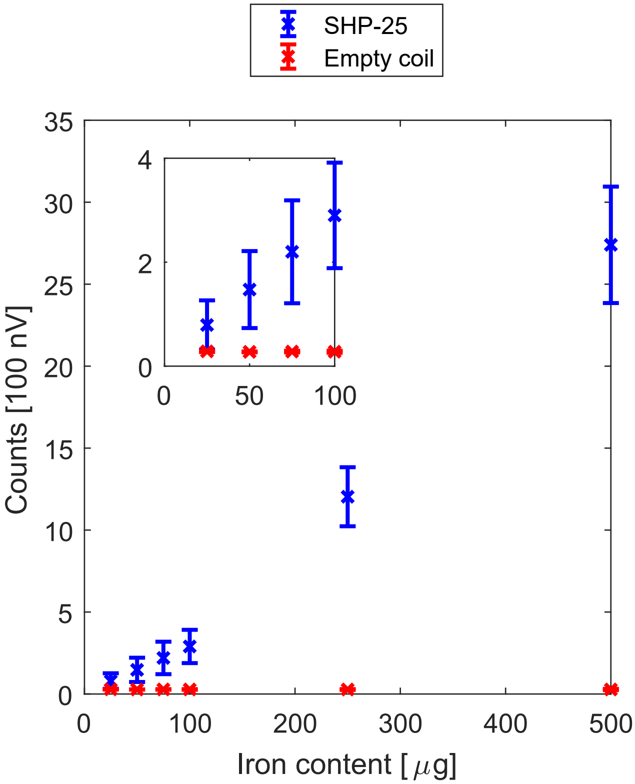

Figure 3.7: Sample measurements showing DiffMag counts for various amounts of SHP-25. Samples were placed directly in front of the detections coils, and detection coils were at a distance of 5 cm from excitation coils, resulting in field strengths of 0.5 mT (AC) and 50 mT (DC). Error bars show ± one standard deviation.

3.4.2 SPION measurements

Static particle measurements are shown in Figure 3.7. SHP-25 can be measured down to 25 μg Fe.

Measurements at various distances to the excitation coils for the SHP-25 sample containing 500 μg Fe are shown in Figure 3.8. Measurements are possible up to 20 cm from the top of the excitation coils.

Figure 3.9 shows DiffMag and AC magnetometry measurements on the SHP-25 sample containing 500 μg Fe. The sample was measured in air, and in proximity to a surgical steel retractor and water. It can be observed that

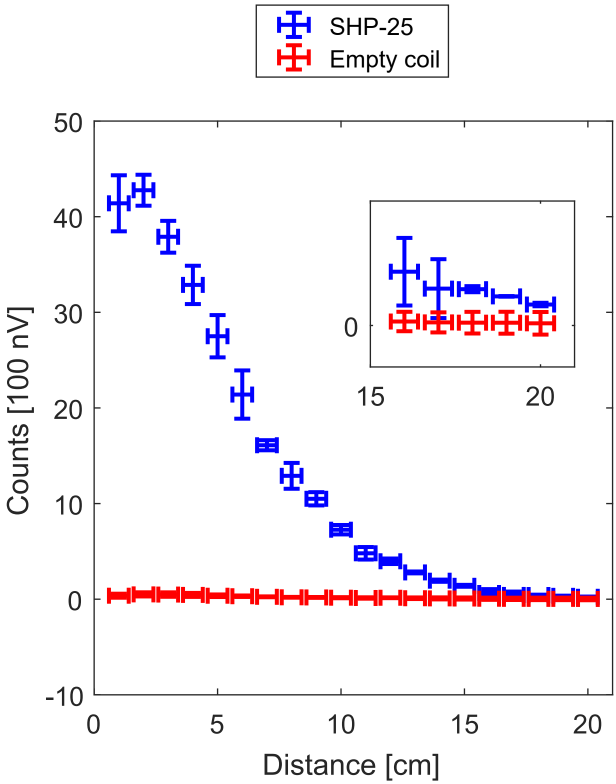

Figure 3.8: DiffMag counts at various distances to the excitation coils. An SHP-25 sample containing 500 μg Fe was placed directly in front of the detection coils. The detection coils and sample were moved away from the excitation coils in steps of 1 cm. Error bars show $\pm$ one standard deviation.

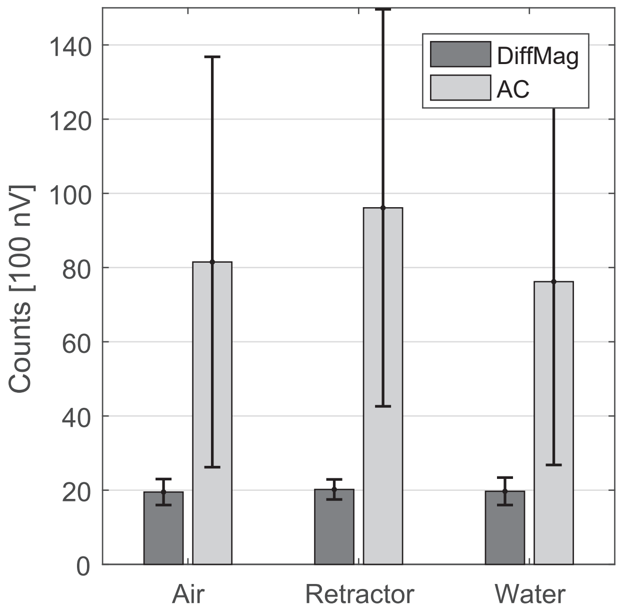

Figure 3.9: DiffMag (left) and AC magnetometry (right) measurements of an SHP-25 sample containing 500 μg Fe. The sample was placed directly in front of the detections coils, and detection coils were at a distance of 5 cm from excitation coils. Measurements were performed in air, with a surgical steel retractor between excitation coil and sample, and with 3 L ($\pm$ 4 cm) water between excitation coil and sample. Error bars show $\pm$ one standard deviation.

DiffMag counts are nearly the same in air and in presence of a surgical steel retractor or water. On the contrary, AC magnetometry counts are increased in presence of a surgical steel retractor, and decreased in presence of water. Furthermore, the standard deviation is much larger in AC magnetometry measurements compared to DiffMag.

3.5 Discussion

Our novel laparoscopic probe for *in vivo* detection of SPIONs has five main advantages. First, it makes use of small field strengths. As a result, energy consumption is limited and handheld detection becomes possible. Second, separation of excitation and detection coils makes it possible to reduce the diameter of the detection coils, while reduction in depth sensitivity is limited. This makes our probe suitable for laparoscopic surgery. The large excitation coils generate a far-reaching excitation field, allowing identification of sentinel nodes at different locations in the body. Third, a feature of our probe is its possibility to cancel the excitation field seen by the detection coils at various distances to the excitation coils. This shows the possibility to balance the probe at any location in the nonuniform excitation field. Consequently, amplification gain can be chosen optimally to measure the tiny magnetic signature of SPIONs.

Fourth, both surgical steel and diamagnetism of water and tissue are not disturbing DiffMag measurements. Figure 3.9 shows that the DiffMag counts are nearly the same when SPIONs are measured in proximity to surgical steel or water. In this experiment, water is used to show the effect of diamagnetism of tissue. In a clinical application, we want to measure a small amount of SPIONs in a large amount of tissue. Therefore, DiffMag's insensitivity to tissue is a big advantage compared to all other probes [14, 15, 12, 16].

The final advantage of our novel probe is DiffMag's robustness for imbalances of the probe. DiffMag is not sensitive to the amplitude of the measured signal, but is a selective measurement for SPIONs. On the contrary, conventional AC magnetometry is not possible when balance of the probe is disturbed. This can be explained by the fact that when balance is disturbed, the amplitude (AC magnetometry) of all blocks of the detected signal increases, whereas the difference in amplitude between the blocks (DiffMag) stays the same. This (in)sensitivity to balance also explains why the standard deviation of the AC magnetometry measurements in Figure 3.9 is much larger compared to the DiffMag measurements. However, active compensation is possible and required for DiffMag, since the sensitive range of the DAQ card is limited. The better the probe is balanced, the smaller the amplitude of the measured signal, enabling a larger amplification gain, making the probe more sensitive.

3.5.1 Performance in relation to clinical needs

Currently, the minimum amount of SPIONs that can be identified with our novel probe contains 25 μg Fe. In the clinical situation, a sentinel node contains 60 – 220 μg Fe [12]. This means that our probe is already sensitive enough to detect sentinel nodes. However, this detection limit of 25 μg Fe was determined for measurements where SPIONs were placed directly in front of the detection coils.

Biot-Savart law is used to predict the maximum detection depth of a sentinel node. Figure 3.7 shows a linear relation between DiffMag counts and amount of iron in the sample. This linear relation is used to calculate the counts induced by a typical sentinel node. The empty coil measurement shown in Figure 3.7 provides the threshold, or minimum number of detectable counts. The depth sensitivity of a sentinel node containing 60 – 220 μg Fe is currently 14 – 24 mm. Reducing noise in the system, as described in section 3.5.2, will improve sensitivity of the probe and consequently the maximum detection depth.

For example, in breast cancer patients, sentinel nodes have a mean depth of 4 cm [11]. However, in laparoscopic surgery sentinel nodes are not measured through the skin, but the probe is placed directly on the fatty tissue containing the lymph nodes[23]. To conclude, the present sensitivity of our probe is already clinically usable.

3.5.2 Improvements before clinical implementation

Although sensitivity of the probe is already clinically usable, the probe can be improved for clinical use in four ways. First, it is essential that movement of detection coils is possible during SPION measurements. This can be achieved by implementation of active compensation in the DiffMag protocol. The signal of one block of the DiffMag sequence will be used to calculate new compensation values and thus to balance the probe. The length of a DiffMag sequence needs to be reduced to enable compensation in real time and faster movement of the probe.

Second, the diameter of the probe must be reduced. For clinical usage it must fit through a standard 12 mm trocar.

Third, sensitivity of the probe can be improved. This will lead to measurement of either a lower quantity of SPIONs, or measuring a sample at a larger distance from the detection coils (measuring nodes that are located deeper in tissue). Currently, there are distortions on the measurement signal. Part of these distortions are caused by the 50 Hz harmonics. This is why we now measure at 2525 Hz instead of 2500 Hz. Furthermore, the power amplifiers seem to introduce noise. We also want to amplify the probe signal directly after the detection coils instead of in the electronics box, to avoid signal loss when the signal is transfered through a cable. Improving these electronics in our setup will improve sensitivity of the probe.

Finally, it would help to make the excitation field more homogeneous. This would make balancing of the probe much easier. If we can achieve a perfectly homogeneous field, the excitation field is the same at every location of the probe. As a result, the field is equal in both detection coils. The coils will be passively balanced, making active compensation less crucial. Another advantage of a homogeneous excitation field is that DiffMag counts are in that case not dependent on the location of the sentinel nodes. Figure 3.8 shows that DiffMag counts decrease when distance to the excitation coils is increased. However, achieving a sufficiently large homogeneous excitation region would require a more complicated setup with large coils, making a surgical procedure more difficult.

It is hard to say how the improvements described in this section will affect the measurements. The theoretical noise limit is the resistance of the detection coils. We are already close to clinical needs, so slight improvements will make this probe usable in the clinic.

3.6 Conclusion

A novel probe for *in vivo* detection of SPIONs has been developed. A unique feature of this probe is mechanical separation of excitation and detection coils. Active compensation was developed and demonstrated, allowing independent movement of the detection coils with respect to the excitation coils. With our current electronics it is possible to measure as little as 25 μg of SPIONs. Furthermore, measurements are successful at various distances from the excitation coils, showing the possibility to move the detection coils. Measurements are successful because we use DiffMag. Distortions in balance of the probe do not influence DiffMag measurements. Finally, both surgical steel and diamagnetism of tissue have minor influence on DiffMag measurements. In conclusion, this paper shows promising first steps towards laparoscopic sentinel node biopsies, since it enables identification of magnetically marked nodes in the diamagnetic human body.

Acknowledgements

Financial support from the Netherlands Organization for Scientific Research (NWO), under the research program Magnetic Sensing for Laparoscopy (MagLap) with project number 14322 is gratefully acknowledged. Furthermore, the authors would like to thank A. Veugelers for creating Figure 3.1, S. Draack for help with creating Figure 3.3, E.R. Nieuwenhuis, A.M. Hoving and M.E. Kamphuis for proofreading and L. Molenaar for discussing content.

Bibliography

[1] A.E. Giuliano and A. Gangi. Sentinel node biopsy and improved patient care. *Breast Journal*, 21(1), 2015.

[2] Bogdan Filip, Marco Scarpa, Francesco Cavallin, Rita Alfieri, Matteo Cagol, and Carlo Castoro. Minimally invasive surgery for esophageal cancer: a review on sentinel node concept. *Surgical Endoscopy*, 28(4):1238–1249, apr 2014.

[3] G. Munbauhal, T. Seisen, F.D. Gomez, B. Peyronnet, O. Cussenot, S.F. Shariat, and M. Rouprêt. Current perspectives of sentinel lymph node dissection at the time of radical surgery for prostate cancer. *Cancer Treatment Reviews*, 50, 2016.

[4] Michael A Liss, Jonathan Noguchi, Hak J Lee, David R Vera, and A Karim Kader. Sentinel lymph node biopsy in bladder cancer: Systematic review and technology update. *Indian journal of urology : IJU : journal of the Urological Society of India*, 31(3):170–175, 2015.

[5] Vahid Reza Dabbagh Kakhki, Reza Bagheri, Shahrzad Tehranian, Pardis Shojaei, Hassan Gholami, Ramin Sadeghi, and David N Krag. Accuracy of sentinel node biopsy in esophageal carcinoma: a systematic review and meta-analysis of the pertinent literature. *Surgery Today*, 44(4):607–619, apr 2014.

[6] David Cibula, Maaike H M Oonk, and Nadeem R Abu-Rustum. Sentinel lymph node biopsy in the management of gynecologic cancer. *Current Opinion in Obstetrics and Gynecology*, 27(1), 2015.

[7] M.C. Darin, N.R. Gómez-Hidalgo, S.N. Westin, P.T. Soliman, P.F. Escobar, M. Frumovitz, and P.T. Ramirez. Role of Indocyanine Green in Sentinel Node Mapping in Gynecologic Cancer: Is Fluorescence Imaging the New Standard? *Journal of Minimally Invasive Gynecology*, 23(2), 2016.

[8] Anabela Rocha, Ana Maria Domínguez, Fabrice Lécuru, and Nicolas Bourdel. Indocyanine green and infrared fluorescence in detection of sentinel lymph nodes in endometrial and cervical cancer staging – a systematic review. *European Journal of Obstetrics & Gynecology and Reproductive Biology*, 206:213–219, 2016.

[9] Gijs H. KleinJan, Nynke S. van den Berg, Oscar R. Brouwer, Jeroen de Jong, Cenk Acar, Esther M. Wit, Erik Vegt, Vincent van der Noort, Renato A. Valdés Olmos, Fijs W.B. van Leeuwen, and Henk G. van der Poel. Optimisation of Fluorescence Guidance During Robot-assisted Laparoscopic Sentinel Node Biopsy for Prostate Cancer. *European Urology*, 66(6):991–998, dec 2014.

[10] M Ahmed, M C L Peek, and M Douek. How can nanoparticles be used in sentinel node detection? *Nanomedicine*, 12(13):1525–1527, 2017.

[11] C. Mathelin, S. Salvador, D. Huss, and J.-L. Guyonnet. Precise localization of sentinel lymph nodes and estimation of their depth using a prototype intraoperative mini γ-camera in patients with breast cancer. *Journal of Nuclear Medicine*, 48(4):623–629, 2007.

[12] Masaki Sekino, Akihiro Kuwahata, Tetsu Ookubo, Mikio Shiozawa, Kaichi Ohashi, Miki Kaneko, Itsuro Saito, Yusuke Inoue, Hiroyuki Ohsaki, Hiroyuki Takei, and Moriaki Kusakabe. Handheld magnetic probe with permanent magnet and Hall sensor for identifying sentinel lymph nodes in breast cancer patients. *Scientific Reports*, 8(1):1195, 2018.

[13] W.A. Waddington, M.R.S. Keshtgar, I. Taylor, S.R. Lakhani, M.D. Short, and P.J. Eli. Radiation safety of the sentinel lymph node technique in breast cancer. *European Journal of Nuclear Medicine*, 27(4):377–391, 2000.

[14] Andreas Karakatsanis, Peer Michael Christiansen, Lone Fischer, Christina Hedin, Lida Pistioli, Malin Sund, Nils Ryegaard Rasmussen, Hjørdis Jørnsgård, Daniel Tegnelius, Staffan Eriksson, Kosmas Daskalakis, Fredrik Wärnberg, Christos J Markopoulos, and Leif Bergkvist. The Nordic SentiMag trial: a comparison of super paramagnetic iron oxide (SPIO) nanoparticles versus Tc99 and patent blue in the detection of sentinel node (SN) in patients with breast cancer and a meta-analysis of earlier studies. *Breast Cancer Research and Treatment*, 157(2):281–294, jun 2016.

[15] A Cousins, G L Balalis, S K Thompson, D Forero Morales, A Mohtar, A B Wedding, and B Thierry. Novel Handheld Magnetometer Probe Based on Magnetic Tunnelling Junction Sensors for Intraoperative Sentinel Lymph Node Identification. *Scientific Reports*, 5:10842, jun 2015.

[16] Hikaru Karo and Ichiro Sasada. Superparamagnetic nanoparticle detection system by using a fundamental mode orthogonal fluxgate (FM-OFG) gradiometer. *AIP Advances*, 7(5):56716, 2017.

[17] J.J. Pouw, D.M.C. Bastiaan, J.M. Klaase, and B. ten Haken. Phantom study quantifying the depth performance of a handheld magnetometer for sentinel lymph node biopsy. *Physica Medica*, 32(7):926–931, 2016.

[18] M. Visscher, S. Waanders, H.J.G. Krooshoop, and B. ten Haken. Selective detection of magnetic nanoparticles in biomedical applications using differential magnetometry. *Journal of Magnetism and Magnetic Materials*, 365:31–39, sep 2014.

[19] S Waanders, M Visscher, R R Wildeboer, T O B Oderkerk, H J G Krooshoop, and B Ten Haken. A handheld SPIO-based sentinel lymph node mapping device using differential magnetometry. *Physics in medicine and biology*, 61(22):8120–8134, nov 2016.

[20] J. Dieckhoff, D. Eberbeck, M. Schilling, and F. Ludwig. Magnetic-field dependence of Brownian and Néel relaxation times. *Journal of Applied Physics*, 119(4), 2016.

[21] Jing Zhong, Meinhard Schilling, and Frank Ludwig. Magnetic nanoparticle thermometry independent of Brownian relaxation. *Journal of Physics D: Applied Physics*, 51(1):015001, dec 2017.

[22] J.J. Pouw, M. Ahmed, B. Anninga, K. Schuurman, S.E. Pinder, M. Van Hemelrijck, Q.A. Pankhurst, M. Douek, and B. ten Haken. Comparison of three magnetic nanoparticle tracers for sentinel lymph node biopsy in an in vivo porcine model. *International Journal of Nanomedicine*, 10:1235–1243, 2015.

[23] Alexander Winter, Tobias Kowald, Tina Susanne Paulo, Philipp Goos, Svenja Engels, Holger Gerullis, Jonas Schiffmann, Ajay Chavan, and Friedhelm Wawroschek. Magnetic resonance sentinel lymph node imaging and magnetometer-guided intraoperative detection in prostate cancer using superparamagnetic iron oxide nanoparticles. *International Journal of Nanomedicine*, Volume 13:6689–6698, oct 2018.

4 | Modelling magnetic nanoparticles using combined Néel and Brownian relaxation

The efficient development and utilisation of magnetic nanoparticles (MNPs) for applications in enhanced biosensing relies on the use of magnetization dynamics, which are primarily governed by the time-dependent motion of the magnetization due to externally applied magnetic fields. An accurate description of the physics involved is complex and not yet fully understood, especially in the frequency range where Néel and Brownian relaxation processes compete. However, even though it is well-known that nonzero, nonstatic local fields significantly influence these magnetization dynamics, the modelling of magnetic dynamics for MNPs often uses zero-field dynamics or a static Langevin approach. In this paper, we develop an approximation to model and evaluate its performance for MNPs exposed to a magnetic field with varying amplitude and frequency. This model was initially developed to predict superparamagnetic nanoparticle behaviour in differential magnetometry applications but it can also be applied to similar techniques, such as magnetic particle imaging and frequency mixing. Our model is based upon the Fokker-Planck equations, for the two relaxation mechanisms. The equations are solved through numerical approximation and they are then combined, while taking into account the particle size distribution and the respective anisotropy distribution. Our model was evaluated for Synomag®-D70, Synomag®-D50 and SHP®-15, which resulted in an overall good agreement between measurement and simulation. The MATLAB-code and experimental data relating to this research are made available: 10.4121/14900565.

The work in this chapter was published as *Modelling of dynamic behaviour in magnetic nanoparticles* by M.T. Rietberg, S. Waanders, M.M. Horstman - van de Loosdrecht, R.R. Wildeboer, B. ten Haken and L. Alic, *Nanomaterials* 11 (12) 3396 (2021). MT Rietberg and the author of this thesis share joint first authorship on the article. The author of this thesis developed the model framework, interpreted the model's results and experimental verification and wrote the initial draft.

4.1 Introduction

Magnetic nanoparticles (MNPs) have become a popular research subject in biomedicine thanks to their high biocompatibility, long shelf life and straightforward logistics when compared to radioactive agents for similar applications. The biomedical application of MNPs ranges from therapy, such as magnetic hyperthermia or targeted drug delivery[1], to diagnostics, where they are applied as contrast agents or tracers[2], or even theranostics [3]. Sensing techniques that employ MNPs include AC magnetometry [4], differential magnetometry [5], magnetic particle spectroscopy (MPS) [6], and magnetic particle imaging (MPI) [7]. All of these techniques rely on targeted magnetic manipulation and accurate acquisition of the dynamic response of an individual MNP. Therefore, an accurate model of the dynamics governing their magnetic properties to enhance the sensing techniques is of vital importance. However, the sensing technologies are often developed sub-optimally regarding magnetization dynamics. The options available for performance optimization include (for example) improved Signal to Noise Ratio (SNR) and optimized excitation sequences. The main goals of the model are:

- Model the behaviour of particles: allow for optimization of particles for a given application without the need for extensive empirical testing.
- Predict a particle's properties, magnetic field properties and environmental parameters, such as viscosity, based on the behaviour of the MNPs.

In recent years, many models have been developed to describe individual aspects of MNP magnetization dynamics under certain magnetic field conditions, including heat dissipation[8], harmonic field response[9, 10, 11, 12], viscosity effects[13], temperature dependence [14], core distribution [15] and damping of the magnetic field[16]. After Brown's seminal paper[17], the characteristic magnetic relaxation times were assessed for a particular case with a constant magnetic field under a step function regime [18]. However, the dynamic behaviour of MNPs in changing magnetic fields is complex, especially in the domain where simultaneous Brownian and Néel processes take place. Brownian relaxation aligns the whole particle with the magnetic field, while Néel relaxation aligns the internal magnetic dipole within the particle. The most frequently used approach to model MNP behaviour under conditions of varying magnetic fields currently involves a phenomenological model of the magnetization response using the steady-state approximation of magnetic particles rotating toward the field's orientation [19, 20, 21, 22]. However, a significant downside to this approach is the fact that particle anisotropy and time delay effects are ignored, therefore this approach often does not hold in practice.

The known relaxation mechanisms (Brownian and Néel) have been modelled using two separate Fokker-Planck equations (FPEs) [18]. The magnetization dynamics of spherical particles with non-critical diameter (meaning that either Brownian or Néel relaxation is dominant) can be described well with these equations, but not of particles with critical diameter (no dominant mechanism) because the FPEs are separate and lack connection. Consequently, this publication presents a practical and effective way of solving these FPEs simultaneously, which accurately describes the nonlinear magnetization dynamics of various superparamagnetic nanoparticles, surprisingly well for non-spherical particles. Its outcomes were validated with magnetometer measurements of three different species of MNP. This model has potential as a tool for use in the design and validation of optimized MNPs for biomedical imaging applications. Furthermore, it enables tailored adjustments of new sensing devices to match the MNP characteristics and consequently to maximize sensitivity.

4.2 Theory

The behaviour of monodisperse (meaning that the mixture contains only MNPs of the same size) superparamagnetic MNPs of non-critical diameter can be described by solving a set of first order non-linear partial differential equations (PDE) that capture Brownian and Néel relaxation. The probability distribution of MNP magnetic moments is defined as $F(x,t)$, where θ is the polar angle between the MNP dipole moment and the direction of the driving magnetic field, $x \equiv \cos\theta$ and t is the time. This set of PDEs (which is approximated by Equations 4.1 and 4.2) is referred to as the Fokker-Planck equations (FPEs) and captures the time evolution behaviour of a probability density function describing transient convection-diffusion with a quadratic space-dependent diffusion and time-dependent driving magnetic field[18].

$$\frac{\partial}{\partial t}F = \frac{1}{2\tau_B}\frac{\partial}{\partial x}\left[(1-x^2)\left(\frac{\partial}{\partial x}F - \xi(t)F\right)\right] \tag{4.1}$$

$$\frac{\partial}{\partial t}F = \frac{1}{2\tau_N}\frac{\partial}{\partial x}\left[(1-x^2)\left(\frac{\partial}{\partial x}F - \xi(t)F - 2\sigma x F\right)\right] \tag{4.2}$$

The driving field $B(t)$ (with varying amplitude and frequency) is described using the effective field parameter $\xi = (m_0/k_BT)B(t)$ and the particle anisotropy constant K is described by the parameter $\sigma = KV_c/k_BT$. Each particle is characterized by a constant magnetic dipole moment with a magnitude of $m_0 = M_sV_c$, with M_s for the saturation magnetization and V_c for the volume of a magnetic core. k_B is Boltzmann's constant, and T is temperature. Furthermore, the relaxation times τ_B and τ_N represent the effective characteristic time constant for Brownian and Néel relaxation, respectively, and read:

$$\tau_B \equiv \frac{3\eta V_h}{k_BT} \tag{4.3}$$

$$\tau_N \equiv \frac{V_c(1+\alpha'^2)M_s}{2\gamma_e\alpha' k_BT} \tag{4.4}$$

Here η is medium viscosity, α' is the damping constant, γ_e is the electron gyromagnetic ratio and V_h is hydrodynamic volume of a particle submerged in medium.

Without a known analytical solution and under an adiabatic approximation, and solving for space-dependent diffusion, the FPEs reduce to the well-known Langevin function [23]. Although this is an elegant solution, the Langevin function does not offer an accurate description of superparamagnetism, especially at a frequency rage where both relaxation processes are equally important. Consequently, the Langevin function fails to accommodate the influence of anisotropy and particle-particle interactions.

Another numerical pathway for solving $F(x,t)$ is by approximating the space-dependent diffusion using Legendre polynomials [10]:

$$F(x,t) = \sum_{l=0}^{\infty} a_l(t)P_l(x) \tag{4.5}$$

Substituting this approximation into Equations 4.1 and 4.2, results in a new set of ordinary differential equations (ODE) for Brownian and Néel relaxation, respectively [18]:

$$\frac{2\tau_B}{l(l+1)}\frac{da_l}{dt} = -a_l + \xi(t)\left[\frac{a_{l-1}}{2l-1} - \frac{a_{l+1}}{2l+3}\right] \tag{4.6}$$

$$\begin{aligned}\frac{2\tau_N}{l(l+1)}\frac{da_l}{dt} =& -a_l + \xi(t)\left[\frac{a_{l-1}}{2l-1} - \frac{a_{l+1}}{2l+3}\right] \\ &+ \sigma\left[\frac{(l-1)a_{l-2}}{(2l-3)(2l-1)} + \frac{la_l}{(2l-1)(2l+1)}\right. \\ &\left. - \frac{(l+1)a_l}{(2l+1)(2l+3)} - -\frac{(l+2)a_{l+2}}{(2l+3)(2l+5)}\right]\end{aligned} \tag{4.7}$$

These ODEs can be used to calculate the time average of x (again, $x \equiv \cos\theta$), which correlates to the magnetic moment:

$$\langle x(t)\rangle = \frac{2}{3}a_1(t) \tag{4.8}$$

$$\frac{d}{dt}M(t) = nM_sV_c\frac{d}{dt}\langle x(t)\rangle \tag{4.9}$$

However, this approach does not combine Brownian and Néel relaxation, and results in two separate magnetization curves. The common practice to omit this problem for static fields and relaxation processes is to consider only the dominant relaxation mechanism[24, 25, 26], or in the critical size range (where both processes are equally contributing) use the geometric mean of both relaxation times [8]. However, neither of these practices reflect reality. Alternative attempts have been made to describe the particle response in terms of a superposition of both relaxation processes[25, 27]. When the applied field changes rapidly (e.g., in case of AC magnetometry), a simple superposition fails to describe the magnetic behaviour of the particles. This can partially be attributed to the inaccurate assumption that these processes are fully independent.

4.3 Methods

4.3.1 MNP samples

Three different types of superparamagnetic MNPs are used to acquire the particle response functions that are necessary to validate the method: Synomag®-D70, Synomag®-D50 (micromod Partikeltechnologie GmbH, Germany) and SHP-15 (Ocean Nanotech, USA). The first two are nanoflower-shaped particles, while the latter is a cluster-typed particle; as can be seen in Figure 4.1. It has to be noted

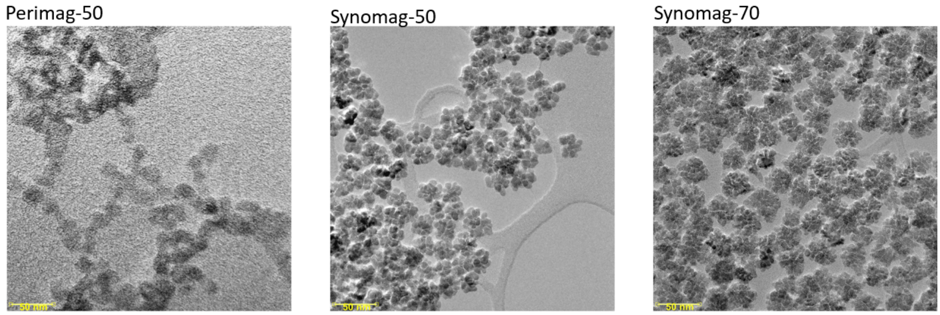

Figure 4.1: TEM micrographs (Philips CM300ST-FEG) of the three nanoparticle species, electron acceleration voltage of 300 kV at a point resolution of 0.2 nm at 300 kV, line resolution of 0.14 nm at 300 kV.

	d_c [nm]	d_h [nm]	K_a [kJ m^{-3} nm^{-1}]	K_b [kJ m^{-3}]	M_s [kA m^{-1}]
Perimag	19 ± 5.7	$d_c + 87$	0.183	5	300
Synomag-D50	24 ± 3.17	$d_c + 42.2$	0.098	9.5	420
Synomag-D70	29 ± 4	$d_c + 37.5$	0.098	9.5	420

Table 4.1: Sample composition. d_c: core diameter [28, 29, 30], d_h: hydrodynamic diameter [28, 29, 30], K_a&K_b: anisotropy constants as denoted in Equation 4.13 (based on [31]) and M_s: saturation magnetization (based on [32])

.

that the model was developed with spherical particles in mind, which does not reflect the real-world properties of the Synomag particles. Table 4.1 gives an overview of the characteristics for all three MNPs, which are polydisperse (meaning that the mixture contains MNPs of varying size, instead of only MNPs with the same size) with an anisotropy constant dependent on size (see Equation 4.13). All of our samples consisted of 140 µg iron dissolved in water, resulting in a total volume of 140 µL contained in glass vials, which was kept at room temperature.

4.3.2 **Data acquisition for experimental observations**

The Particle Response Function (PRF) was acquired using the characterization mode of the SuperParamagnetic Quantifier (SPaQ), which is an in-house developed magnetometer utilising a homogeneous magnetic field[33]. PRFs were assessed by exposing the samples to a continuous alternating magnetic field ($B_{ac} = 1.3mT$, frequency = 2.5 kHz), with an increasing offset field B_+ ranging from -13 to $13mT$:

$$B(t) = B_{AC}\sin(2\pi ft) + \dot{B}_+ t \tag{4.10}$$

The subsequent magnetization signal is acquired by a set of gradiometric coils with a sensitivity of $S_{det} = 37.8mT/A$, which leads to an induced voltage $U_{det}(t)/S_{det} = -\frac{d}{dt}M(t)$.

4.3.3 **Model**

We approach the fact that we are dealing with two separate relaxation mechanisms by initially considering both processes to operate independently. Since a magnetometer measures the *rate of change* of the magnetization, one observes the sum of two orthogonal rotations. Following the Legendre approximations (as described in Eqs 4.6 and 4.7) [18, 34], the contribution of Néel and Brownian relaxation processes to the response of the MNPs to an externally applied magnetic field is assessed by:

$$\frac{d}{dt}M(t) = \sqrt{\left(\frac{d}{dt}M_{Brown}\right)^2 + \left(\frac{d}{dt}M_{Néel}\right)^2} \tag{4.11}$$

The initial theoretical assumption of monodispersity in MNPs does not match the current reality of commercially available polydisperse MNPs. Therefore, to model particle response function accurately (solution of Equation 4.11), the particle size distribution needs to be taken into account. Consequently, we approximate the polydispersity in core diameters d_c by a normal distribution, which is detailed in Table 4.1. For numerical purposes, this distribution is discretized into an increasing number of bins until the resulting individual MNPs response (again, solution of Equation 4.11) stabilizes, which means that a further increase in bin density does not noticeably change the solution. Finally, the PRF is defined as the weighted average of these responses according to the discretized normal distribution.

Brownian relaxation influences the Néel relaxation by orienting the MNPs along the direction of the applied magnetic field [35, 36]. If Brownian relaxation is not possible (e.g., when particles are trapped in a medium or tissue), then Brownian relaxation is prohibited. Depending on the orientation of the magnetic easy axes of the particles suspended in the sample under investigation, this effect alters the Néel relaxation behavior of the particles if their anisotropy is not equal to unity (i.e., they deviate from perfect spherical symmetry). Following initial research by Shliomis et al. [37], this effect is modelled by an effective anisotropy constant as an energy term K_{eff}, which is composed of both longitudinal and transverse anisotropy energies. Assuming the potential landscape as $U = K \sin^2 \theta$, then we have $U_{\parallel} = K$ in the longitudinal case and $U_{\perp} = 0$ for both transverse orientations. This results in an effective anisotropy constant:

$$K_{\text{eff}} = \frac{1}{3} K_{\parallel} + \frac{2}{3} K_{\perp} = \frac{1}{3} K \tag{4.12}$$

Considering that the anisotropy constant changes with the particle core size [38], a polydisperse sample cannot be modelled using only one anisotropy constant. Therefore, a relation is proposed, which results in a different anisotropy constant for each core size:

$$K = K_a d_c + K_b \tag{4.13}$$

K_a and K_b are fit parameters for known anisotropy constants for certain diameters. The resulting K can be filled into Equation 4.12 to get the effective constant. While Equation 4.13 is not a perfect solution due to the assumption of linear relation (which would determine the anisotropy constant for every particle size), it is an improvement from the same constant for all particle sizes.

To evaluate the formulated magnetization dynamics (Equation 4.11) and to elaborate on the regimes in which either relaxation mechanism might dominate, we compute the resultant magnetization curves for monodisperse nanoparticle samples of selected core sizes (d_c =

	Perimag®		Synomag®-D50		Synomag®-D70	
	FWHM (% diff)	MoR	FWHM (% diff)	MoR	FWHM (% diff)	MoR
Model	-1.03	0.002	-47.22	0.217	-24.46	0.105
Langevin	54.52	0.094	-56.05	0.284	-31.28	0.130

Table 4.2: Quantification of the Goodness of Fit of Figure 4.3, based on difference in Full Width Half Maximum from the experimental data and the Mean of absolute Residuals in the FWHM window

$10nm, 18nm, 26nm$). This was visualized by means of their PRFs, which are similar to the derivative of the magnetization curve or the point spread function in MPI. This denotes the sample's signal amplitude as a function of the applied field magnitude.

4.3.4 Model validation

Our model is validated by comparing the results to a classical solution of FPE (using the Legendre polynomials) and experimental observations. Three species of MNPs, namely Synomag®-D70, Synomag®-D50 and SHP-15, were evaluated for their magnetic performance using their PRF. This was done three times and then averaged to filter unwanted fluctuations. These results were compared with a numerical evaluation of the model that we introduced earlier. It is common practice to set the damping constant to 0.1, and work with a ferrofluid viscosity of $\eta = 1.0049$ mPa s; the other parameters are defined in Table 4.1. The model was evaluated in MATLAB (2021a, MathWorks, Natick, USA) using the *ode15s* subroutine, a variable-step, variable-order solver for stiff differential equations based on the numerical differentiation formulas. The Legendre expansion converges fairly rapidly, and the set of ODEs was evaluated up to the 60th coefficient.

To quantify the goodness of fit, a Full Width Half Maximum (FWHM) and a Mean of absolute Residuals (MoR) are used. The FWHM is an important characteristic in MPI because it denotes the spatial resolution. The MoR is the mean of the absolute difference inside the FWHM-window. Thus, the difference of the experimental data and the model result was calculated inside the FWHM window. The absolute value of these differences was averaged to get the MoR: $(\sum_n |M(B_n) - E(B_n)|)/n$, where M is the model result and E is the experimental data.

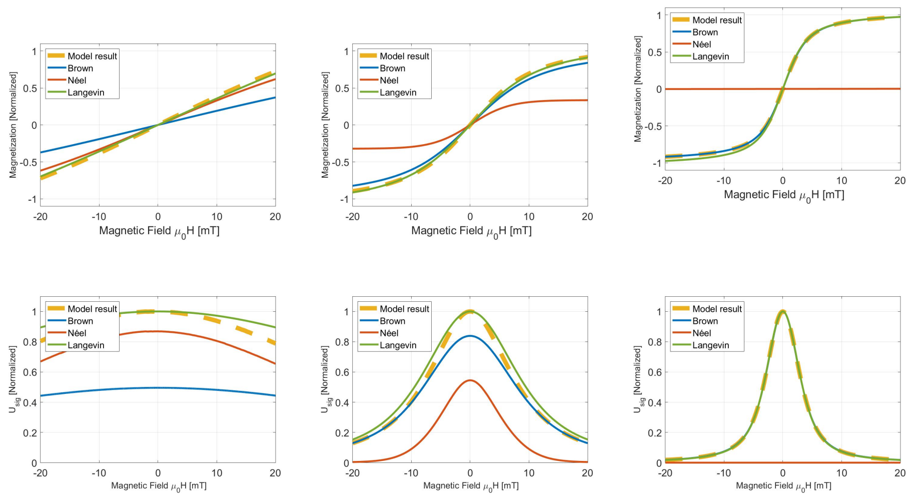

Figure 4.2: Magnetization curves, their numerical derivatives and corresponding relaxation times as a function of magnetic field for monodisperse particles, which are obtained from numerical evaluation of the Brownian and Néel FPEs for 10 nm (left), 18 nm (middle) and 26 nm (right) particles. Simulation parameters: $K = 20$ kJ/m^3, $d_h = d_c + 12$ nm, $T = 300$ K, $\alpha' = 0.1$, $\eta = 1.0049$ mPas, $M_s = 300$ kJ/m^{3}T.

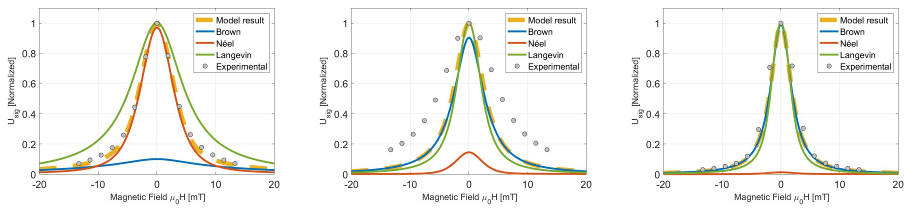

Figure 4.3: Particle Response Functions (experimental and simulated) for three particle-types under application of a 2.5 kHz, 1.3 mT/μ_0 AC field, $\alpha' = 0.1$, $\eta = 1.0049$ mPas, the particles' characteristics can be found in Table 4.1. Left: Perimag®, T: 298 K, bins: $\{10, 11, \ldots, 25\}$ nm. Middle: Synomag®-D50, T: 267K, bins: $\{14, 15, \ldots, 34\}$ nm. Right: Synomag®-D70, T: 267K, bins: $\{14, 15, \ldots, 34\}$ nm

Results

4.4.1 Numerical modelling of Brownian and Néel dominated M-H curves

To explore the boundaries of the developed model, we calculate the behaviour of particles with characteristics that would, under normal circumstances, lead to either Brownian or Néel dominated magnetization behaviour. Figure 4.2 illustrates the magnetization curves for iron oxide particles of different core diameters (10nm, 18nm and 26nm) and constant coating thickness (6nm). As expected, the largest particle shows a magnetization curve corresponding to Brownian dominated relaxation, while the smallest particle shows a magnetization curve corresponding to Néel behaviour. However, the 18nm particle does not have a dominant relaxation mechanism and shows competing behaviour of both relaxation mechanisms. We observe Néel behaviour for low offset field (B^+) values, whereas Brownian relaxation dominates for higher fields. This relates well to observations by Deissler *et al*, who also showed a transition from Néel to Brownian behaviour for increasing field strengths.

4.4.2 Experimental verification of particle response functions

The experimental and numerical results for Perimag®, Synomag®-D50 and Synomag®-D70 are shown in Figure 2. The data are normalized with respect to the largest value to assess shape similarity. Quantification of the Goodness of Fit can be seen in Table 4.2. Overall, we observe a good agreement between the shape predicted by the simulations and the experimental results, showing predominantly Brownian relaxation in the case of Synomag®-D70 and Néel relaxation for Perimag®. Furthermore, the Langevin function fails to adequately predict the shape of the PRF. For the critical case of Synomag®-D50, the model shows potential for improvement but still surpasses the Langevin equation.

4.5 Conclusions and Discussion

In this work, we explored the magnetization dynamics of a variety of MNPs. The FPEs pertaining to Brownian and Néel relaxation were solved by means of their Legendre approximations. A strong point of our model is the fact that it includes the effects of polydispersity and the resulting anisotropy. Our model also demonstrates the impact of both relaxation mechanisms on the magnetization dynamics of particles simultaneously. We observe a deviation from the commonly used Langevin solution for the magnetic behaviour of MNPs, even in the case of larger particles that predominantly relax through Brownian relaxation. For all cases, it was observed that the adiabatic approximation (the Langevin equation) is not valid because of the finite Brownian relaxation time, even at the relatively low frequency of 2.5 kHz and low excitation field strengths. Moreover, we found that the PRF shape of MNPs in the critical size range is well predicted by a combined model that takes both Brownian an Néel relaxation into account. The difference between the model result and the experimental data might be explained by the assumption of a spherical particle, as the Synomag particles are instead flower-shaped. Furthermore, Brownian relaxation dominates in the high field range, while Néel relaxation describes the low-field regime quite well. Keeping this effect in mind, a close look at the PRFs obtained by Arami *et al.*[39] leads to a similar conclusion. Here, an increase in the steepness of PRFs was observed for increasing viscosity, while particles suspended in chloroform (lowering the viscosity) show a much flatter PRF, all else being equal.

The results presented in this work are qualitatively well described by a system of independent Brownian and Néel relaxation, despite the inevitable simplification of details such as Brownian alignment, which influences the Néel process. For example, the Brownian relaxation process influences the Néel relaxation through alignment of the particle's magnetic easy axis, which is hindered when particles are immobilized. This effect can be easily corrected for in this extreme case by defining an effective anisotropy constant for immobilized particles with randomly oriented easy axes. It would be most interesting to measure the PRFs for particles immobilized under application of a strong external magnetic field and for particles immobilized in zero field, and then verify this hypothesis.

Following the analogy used by Weizenecker *et al* [40], our model could likely be improved by modelling with the coupled FPE instead of the currently used decoupled FPEs. The existing model is based on a coupled Fokker-Planck equation but has not yet been validated through experimental data. Moreover, as noted in previous sections, the linear relation between anisotropy and (only) the particle size is limited. This imperfect solution is a good start however, because particle size is one of the factors that affect the anisotropy constant the most.

We must also comment that the experimental variation in particle parameters d_c, d_h, K and M_s, as well as the inherent uncertainty in iron concentration, complicates truly quantitative matching between model and experiment. This deserves more attention, especially in view of the considerable variety in the reported anisotropy constants K in the literature [28, 41, 31, 42]. The current values for K_a and K_b are based on K of Ludwig et al., because this value lies in the middle of the range found in literature and fits our results the best. Nevertheless, by means of designing new or improving existing particles, it is possible to fine-tune the desired PRF parameters (e.g. FWHM) because the connection between particle composition and magnetization dynamics can be better understood through studying this model. This will in turn improve the quality of biomedical applications.

4.6 Acknowledgement

Frans Tichelaar at the Quantum Nanoscience department, Kavli Institute of Nanoscience, Delft University of Technology, is acknowledged for the TEM measurements.

Bibliography

[1] Q A Pankhurst, J Connolly, S K Jones, and J Dobson. Applications of magnetic nanoparticles in biomedicine. *Journal of Physics D: Applied Physics*, 36(13):R167–R181, jun 2003.

[2] Kannan M. Krishnan. Biomedical nanomagnetics: A spin through possibilities in imaging, diagnostics, and therapy. *IEEE Transactions on Magnetics*, 46(7):2523–2558, 2010.

[3] Dongwon Yoo, Jae-Hyun Lee, Tae-Hyun Shin, and Jinwoo Cheon. Theranostic magnetic nanoparticles. *Accounts of Chemical Research*, 44(10):863–874, 2011. PMID: 21823593.

[4] Michael Douek, Joost Klaase, Ian Monypenny, Ashutosh Kothari, Katalin Zechmeister, Douglas Brown, Lynda Wyld, Philip Drew, Hans Garmo, Olorunsola Agbaje, Quentin Pankhurst, Bauke Anninga, Maarten Grootendorst, Bennie Ten Haken, Margaret a Hall-Craggs, Arnie Purushotham, and Sarah Pinder. Sentinel Node Biopsy Using a Magnetic Tracer Versus Standard Technique: The SentiMAG Multicentre Trial. *Annals of surgical oncology*, pages 1237–1245, 2013.

[5] M. Visscher, S. Waanders, H.J.G. Krooshoop, and B. ten Haken. Selective detection of magnetic nanoparticles in biomedical applications using differential magnetometry. *Journal of Magnetism and Magnetic Materials*, 365:31–39, 2014.

[6] Kai Wu, Diqing Su, Renata Saha, Jinming Liu, Vinit Kumar Chugh, and Jian-Ping Wang. Magnetic particle spectroscopy: A short review of applications using magnetic nanoparticles. *ACS Applied Nano Materials*, 3(6):4972–4989, 2020.

[7] Bernhard Gleich and Jürgen Weizenecker. Tomographic imaging using the nonlinear response of magnetic particles. *Nature*, 435(7046):1214–1217, jun 2005.

[8] R.E. E Rosensweig. Heating magnetic fluid with alternating magnetic field. *Journal of Magnetism and Magnetic Materials*, 252(0):370–374, 2002.

[9] B U Felderhof and R B Jones. Mean field theory of the nonlinear response of an interacting dipolar system with rotational diffusion to an oscillating field. *Journal of Physics: Condensed Matter*, 15(23):4011–4024, 2003.

[10] B U Felderhof and R B Jones. Nonlinear response of a dipolar system with rotational diffusion to an oscillating field. *Journal of Physics: Condensed Matter*, 15(15):S1363–S1378, 2003.

[11] Adam M. Rauwerdink and John B. Weaver. Viscous effects on nanoparticle magnetization harmonics. *Journal of Magnetism and Magnetic Materials*, 322(6):609–613, 2010.

[12] Adam M Rauwerdink and John B Weaver. Harmonic phase angle as a concentration-independent measure of nanoparticle dynamics. *Medical physics*, 37(6):2587–2592, 2010.

[13] Takashi Yoshida, Shi Bai, Aiki Hirokawa, Kazuhiro Tanabe, and Keiji Enpuku. Effect of viscosity on harmonic signals from magnetic fluid. *Journal of Magnetism and Magnetic Materials*, 380:105–110, 2015.

[14] Tamara Kahmann, Enja Laureen Rösch, Keiji Enpuku, Takashi Yoshida, and Frank Ludwig. Determination of the effective anisotropy constant of magnetic nanoparticles – comparison between two approaches. *Journal of Magnetism and Magnetic Materials*, 519:167402, 2021.

[15] Zhongzhou Du, Yi Sun, Oji Higashi, Yuki Noguchi, Keiji Enpuku, Sebastian Draack, Klaas-Julian Janssen, Tamara Kahmann, Jing Zhong, Thilo Viereck, Frank Ludwig, and Takashi Yoshida. Effect of core size distribution on magnetic nanoparticle harmonics for thermometry. *Japanese Journal of Applied Physics*, 59(1):010904, dec 2019.

[16] T.L. Gilbert. Classics in Magnetics A Phenomenological Theory of Damping in Ferromagnetic Materials. *IEEE Transactions on Magnetics*, 40(6):3443–3449, 2004.

[17] William Fuller Brown. Thermal fluctuations of a single-domain particle. *Physical Review*, 130(5):1677–1686, 1963.

[18] Robert J. Deissler, Yong Wu, and Michael A. Martens. Dependence of brownian and néel relaxation times on magnetic field strength. *Medical Physics*, 41(1):012301, 2014.

[19] M. Visscher, S. Waanders, H.J.G. Krooshoop, and B. ten Haken. Selective detection of magnetic nanoparticles in biomedical applications using differential magnetometry. *Journal of Magnetism and Magnetic Materials*, 365:31–39, 2014.

[20] R. Matthew Ferguson, Amit P. Khandhar, and Kannan M. Krishnan. Tracer design for magnetic particle imaging (invited). *Journal of Applied Physics*, 111(7):07B318, 2012.

[21] J Weizenecker, J Borgert, and B Gleich. A simulation study on the resolution and sensitivity of magnetic particle imaging. *Physics in Medicine and Biology*, 52(21):6363–6374, oct 2007.

[22] Laura R. Croft, Patrick W. Goodwill, and Steven M. Conolly. Relaxation in x-space magnetic particle imaging. *IEEE Transactions on Medical Imaging*, 31(12):2335–2342, 2012.

[23] Daniel B. Reeves and John B. Weaver. Approaches for modeling magnetic nanoparticle dynamics. *Critical Reviews™ in Biomedical Engineering*, 42(1):85–93, 2014.

[24] P C Fannin and S W Charles. The study of a ferrofluid exhibiting both Brownian and Neel relaxation. *Journal of Physics D: Applied Physics*, 22(1):187–191, 2000.

[25] R Kötitz, W Weitschies, L Trahms, and W Semmler. Investigation of Brownian and Neel relaxation in magnetic fluids - Condens. Matter. *Journal of Magnetism and Magnetic Materials*, 201:102—-104(3), 1999.

[26] S. Draack, T. Viereck, F. Nording, K.-J. Janssen, M. Schilling, and F. Ludwig. Determination of dominating relaxation mechanisms from temperature-dependent magnetic particle spectroscopy measurements. *Journal of Magnetism and Magnetic Materials*, 474:570–573, 2019.

[27] R. Kötitz, W. Weitschies, L. Trahms, W. Brewer, and W. Semmler. Determination of the binding reaction between avidin and biotin by relaxation measurements of magnetic nanoparticles. *Journal of Magnetism and Magnetic Materials*, 194(1):62–68, 1999.

[28] Dietmar Eberbeck, Cindi L. Dennis, Natalie F. Huls, Kathryn L. Krycka, Cordula Gruttner, and Fritz Westphal. Multicore magnetic nanoparticles for magnetic particle imaging. *IEEE Transactions on Magnetics*, 49(1):269–274, 2013.

[29] Kalthoum Riahi, Max T. Rietberg, Javier Perez y Perez, Corné Dijkstra, Bennie ten Haken, and Lejla Alic. Effect of changing iron content and excitation frequency on magnetic particle imaging signal: A comparative study of synomag® nanoparticles. *International Journal of Chemical and Materials Engineering*, 15(5):109 – 112, 2021.

[30] Kalthoum Riahi, Melissa M. van de Loosdrecht, Lejla Alic, and Bennie ten Haken. Assessment of differential magnetic susceptibility in nanoparticles: Effects of changes in viscosity and immobilisation. *Journal of Magnetism and Magnetic Materials*, 514:167238, 2020.

[31] Frank Ludwig, Hilke Remmer, Christian Kuhlmann, Thilo Wawrzik, Hamed Arami, R. Mathew Ferguson, and Kannan M. Krishnan. Self-consistent magnetic properties of magnetite tracers optimized for magnetic particle imaging measured by ac susceptometry, magnetorelaxometry and magnetic particle spectroscopy. *Journal of Magnetism and Magnetic Materials*, 360:169–173, 2014.

[32] Richard Mathew Ferguson, Amit P. Khandhar, Hamed Arami, Loc Hua, Ondrej Hovorka, and Kannan M. Krishnan. Tailoring the magnetic and pharmacokinetic properties of iron oxide magnetic particle imaging tracers. *Biomedizinische Technik/Biomedical Engineering*, 58(6):493–507, 2013.

[33] M. M. Van De Loosdrecht, S. Draack, S. Waanders, J. G.L. Schlief, H. J.G. Krooshoop, T. Viereck, F. Ludwig, and B. Ten Haken. A novel characterization technique for superparamagnetic iron oxide nanoparticles: The superparamagnetic quantifier, compared with magnetic particle spectroscopy. *Review of Scientific Instruments*, 90(2):024101, feb 2019.

[34] Michael Martens, Robert Deissler, Yong Wu, Bauer Lisa, Zhen Yao, Brown Robert, and Griswold Mark. Modeling the Brownian relaxation of nanoparticle ferrofluids: Comparison with experiment. *2013 International Workshop on Magnetic Particle Imaging, IWMPI 2013*, 022303, 2013.

[35] J Weizenecker, J Borgert, and B Gleich. A simulation study on the resolution and sensitivity of magnetic particle imaging. *Physics in medicine and biology*, 52(21):6363–6374, 2007.

[36] Jürgen Weizenecker, Bernhard Gleich, Jürgen Rahmer, and Jörn Borgert. Micro-magnetic simulation study on the magnetic particle imaging performance of anisotropic mono-domain particles. *Physics in Medicine and Biology*, 57(22):7317–7327, 2012.

[37] Mark I. Shliomis and V. I. Stepanov. Theory of the dymamic susceptibility of magnetic fluids, 1994.

[38] Abdel-Fatah Lehlooh, Sami H. Mahmood, and John M. Williams. On the particle size dependence of the magnetic anisotropy energy constant. *Physica B: Condensed Matter*, 321(1):159–162, 2002. Proceedings of the Second Regional Conference on Magnetic and Sup erconducting Materials.

[39] Hamed Arami, R M Ferguson, Amit P Khandhar, and Kannan M Krishnan. Size-dependent ferrohydrodynamic relaxometry of magnetic particle imaging tracers in different environments. *Medical Physics*, 40(7):071904, 2013.

[40] Jürgen Weizenecker. The Fokker-Planck equation for coupled Brown-Néel-rotation. *Physics in Medicine and Biology*, 63(3):035004, feb 2018.

[41] P.C Fannin. Magnetic spectroscopy as an aide in understanding magnetic fluids. *Journal of Magnetism and Magnetic Materials*, 252:59–64, 2002. Proceedings of the 9th International Conference on Magnetic Fluids.

[42] Frank Ludwig, Christian Kuhlmann, Thilo Wawrzik, Jan Dieckhoff, Aidin Lak, Amit P. Kandhar, Richard Matthew Ferguson, Scott J. Kemp, and Kannan M. Krishnan. Dynamic magnetic properties of optimized magnetic nanoparticles for magnetic particle imaging. *IEEE Transactions on Magnetics*, 50(11):1–4, 2014.

5 | Discussion and outlook

Wrapping up, this thesis has described the development of Differential Magnetometry and a few of its implementations. Initially designed to solve a clinical need for a selective, radiation-free alternative to the established radioisotope SLNB procedure in breast cancer, DiffMag has developed into a versatile platform technology with promising applications. In this final chapter, I discuss my findings on the development of the DiffMag technology, and discuss its limitations and potential for further development.

5.1 Conclusions

When we summarize the results presented in this thesis, it follows the complete development of a particle-detector system for biomedical applications. We have established the DiffMag protocol selectively filters out the linear magnetic signal, isolating the nonlinear signal which uniquely identifies the SPIO nanoparticles from their (diamagnetic) background. Additionally, because the magnetic signal from surgical steels in the employed field range is linear as well, these contributions are filtered out, provided movement of the probe is slow compared to the processing speed of the DiffMag system.

Following this, we tackle one of the main disadvantages of a Faraday-based detection system, which is the fact that its maximum attainable detection depth is limited by the diameter of the coils. Because of its differential nature, we can split the excitation and detection coils of the DiffMag probe, which alleviates this downside. As a proof of concept, we've shown this works, which is essential for applications that require small diameter probes, like laparoscopy. Further improvements to processing speed and excitation field homogeneity will improve accuracy and detection depth.

Finally, the system relies on an optimally tuned tracer-detector system. Therefore, we developed an intuitive model that allows us to optimize a tracer for a certain set of excitation parameters, both field strength and frequency. We have shown good agreement between model and experimental verification, with small discrepancies mostly caused by approximating the complex particle structure (nanoflowers, for example) by simple spheres.

Here, we summarize the obtained results from all three components - DiffMag principle development, probe developments and the particle magnetization model.

5.1.1 **DiffMag**

In *Chapter 2* we documented the development of a handheld DiffMag device for intraoperative use. The clinical case that was considered concerned breast cancer - meaning the area of interest for the probe to work in is primarily the axilla. The geometrical constraints of this case were such that a small diameter probe was required. As the field penetration of a Faraday system is strongly dependent on the excitation coil diameter, measurement depth is very limited in this case. However, probes of similar geometries have shown good clinical results despite this drawback.

The resilience of the DiffMag probe with regards to the presence of metal is noteworthy, and a big advantage compared to other magnetometry techniques. This filtering effect works because the field at which magnetic saturation for these materials occurs lies much higher than that of the SPIO nanoparticles, and the magnetic behavior of the surgical steels can be considered linear. However, even though we have shown the method in itself works, its efficacy during movement is limited due to the speed of signal processing. Even though the magnetization signal is linear and nature and thus is filtered out by DiffMag, it still induces a large current before processing, and thus potentially clips the input range of the detection coils. This can be countered by effective compensation of the induced linear signal, but this requires near real-time signal processing. It is strongly recommended to move signal processing into the analog domain before data acquisition (which is currently the limiting factor with regards to speed), or move it to a dedicated chip like an FPGA. With faster acquisition and processing, dynamic compensation of the varying linear contribution to the signal will be possible.

Regarding the separation of excitation and detection coils - we have shown that it is still possible to detect relevant amounts of SPIO nanoparticles, even when the mutual induction between excitation and detection coils varies (by physically allowing them to move relative to each other). This is possible due to the differential nature of our procedure.

5.1.2 **Particle design and evaluation**

Obviously, the detector is only half of the system here. In *Chapter 4* I described an intuitive model we use to quickly assess a particle's relevant properties for use with a DiffMag detector. Studying this model, we come to the conclusion that a traditional Langevin only solution to the Brownian Fokker-Planck equation is insufficient, and a coupling between both Fokker-Planck equations is required, because both relaxation channels aren't independent of each other. For small particles, Neèl relaxation dominates, whereas for larger (clusters of) particles, the Brownian channel completely determines the particle ensemble's magnetic performance. However, in the critical range of 15-25nm, both channels influence each other and contribute to the resultant signal. We realize our approach is intuitive at best and not exactly representative of the real-world physics going on, as the coupling in our case is only made through the anisotropy constant K. Successful approaches to couple both F-P equations have been explored, but are much more computationally intensive. *Main point: Brownian relaxation improves Neel relaxation by aligning easy axis of the particle with the applied magnetic field. Concurrent solution of both F-Ps is hard, so we incorporate this effect by lowering the anisotropy constant.*

5.1.3 **Tracer availability**

In an ideal world, we would be able to design, produce and use an optimized particle and detector combination. In reality however, very few tracer materials are available in clinically relevant quantities, and even fewer have managed to navigate the (rightfully so) complex certification pathways, and have obtained either FDA or CE clearance. This is a definite risk for clinical acceptance and uptake of detection methods relying on these tracers, and new CE regulations have definitely not improved the success rate of new products so far.

5.1.4 **Application aspects - clinical considerations**

When thinking about applying DiffMag in a clinical context - like the SLNB procedure, it is important to consider the up and downsides of both DiffMag and its existing and potential competitors. By combining the selectivity of a radioisotope-based detection procedure with the safety and logistical advantages of conventional magnetic tracers, we aimed to combine the best of both worlds. However, as we showed in this thesis, our approach has downsides as well. These mainly concern, besides the earlier addressed limitations around probe diameter and detection depth and speed, electromagnetic compatibility with other equipment in the surgical area. Given the electronically noisy and complex surroundings in the OR, and to prevent problematic interference with the normal operation of this equipment (EEG, ECG, for example), this aspect deserves more attention. Even though our solution was designed with EMC compatibility and the ICNIRP guidelines in mind, testing in a real world or realistically simulated environment is essential to prove the solution's efficacy and safety.

During the development of the first DiffMag probes, clinicians have been involved from the get go. We believe that design and implementation of a new medical device needs to be done in close collaboration with the eventual end user, as early as possible. Therefore, we believe and have received feedback that the device has a usable form factor for a surgeon, and performs similarly to the current gold standard in terms of user interface and user experience. For new applications, it is vital to reassess the exact needs in terms of UI and UX together with the intended end users.

5.2 Outlook

At the beginning of this thesis, I mentioned the somewhat lackluster uptake of magnetic techniques in medicine, outside of shielded rooms at least. We strongly believe that by designing a robust measurement technique, combined with state of the art nanoparticle technology, we are slowly but surely able to move out of the magnetically shielded room, and into, in this case, the operating theatre. Many challenges lie ahead to bring the DiffMag principle from a proof of concept stage to a mature technology. Subsequent research projects following mine have already shown promising results, both in maturing the measurement concept and in broadening the application spectrum from breast cancer, to head & neck carcinoma and laparoscopy. Whilst obviously we focus on magnetic techniques in this thesis, in the end the only thing that matters is the optimal implementation of a (diagnostic) devices is the optimal solution that benefits the patient most. Sometimes that will be a magnetic technique, in other situations a nuclear medicine approach may be more beneficial. In the end, the device ought to fit the problem at hand, and not the other way around.

Coming back to our stated intention in the introduction of this thesis, our aim was to develop a practical device that would allow us to move magnetic detection techniques out of the shielded environment that limits its uptake in medical practise. By implementing Differential Magnetometry in a small, handheld device, with its active compensation allowing us to filter out unwanted signals from the environment like the human body and surgical instruments, we have shown that it is definitely possible to use sensitive, selective magnetometry without the need for shielded rooms and cumbersome hardware.

Summary

The implementation of magnetic detection techniques in clinical practice has long lagged behind developments in society as a whole. Whilst techniques like magnetic resonance imaging and (to a lesser extent) MEG/MCG have been succesfully introduced, use of magnetic techniques for diagnostics and treatment has always been limited to well controlled, shielded environments. In this thesis, we describe the development of a sensitive and specific method to use magnetic nanoparticles for diagnostics and localization, without the need for shielded surroundings. This opens up a world of new applications for magnetic detection, ranging from intraoperative detection of sentinel lymph nodes to tracking and tracing of stem cell therapies, to navigation applications.

Differential Magnetometry

In **chapter 2**, we introduce the concept of Differential Magnetometry. By exciting a sample containing superparamagnetic iron oxide nanoparticles (SPIONs) with an induction coil generating an alternating magnetic field, we magnetize the particles. This magnetization is measured by a pair of detection coils. If we now periodically add a static magnetic field to the excitation, we alter the magnetic response of the particles, because the magnetization dynamics of these particles are strongly nonlinear. By determining the difference between these two magnetization signals, we obtain a specific particle signal, which contrasts with the predominantly linear magnetic properties of tissue and surgical instruments, in this field range. In this chapter, we illustrate how the time derivative of the magnetization changes as the magnetization is pushed towards saturation by the applied DC offset field.

The principle of Differential Magnetometry was implemented in a handheld probe, intended for intraoperative detection of the sentinel lymph node during breast cancer surgery. This application forms a

formidable challenge for magnetic techniques, as demands on sensitivity and selectivity are high, and the injected dose needs to be as low as possible to prevent post surgical sideeffects like skin staining and MRI artefacts. Additionally, emitted power of the coils is limited to prevent tissue heatup and other effects like described in the ICNIRP guidelines on non ionizing radiation protection. Whilst conventional magnetometers, explored for this type of application, have issues balancing out the effects of a varying background susceptibility (due to different tissue oxygenation, which is slightly paramagnetic, for example), and metallic surgical instruments, DiffMag is robust against these artifacts, provided the measurement electronics are fast enough to compensate in real time for the changing induced signal. In this chapter, we outlined the clinical requirements for this application, and how they translate into a first prototype probe and electronics combination. The probe consists of coaxial pairs of excitation and detection coils, with a few windings of compensation coil wound around the excitation coil for real-time adjustment of the excitation parameters. The excitation coils are driven by a current controlled power amplifier, which is controlled by MATLAB through a high-speed DAQ system. Following the detection coils, a lownoise preamplifier forms the final element of the probe. An instrumentation amplifier takes the measured signal and feeds it into the processing DAQ. The DiffMag signal analysis and processing are all performed in MATLAB. All characterization measurements were performed using samples of the well known MRI contrast agent *Resovist*. Probe operation was evaluated by measuring its dose-response curve, lateral and depth sensitivity. Furthermore, we show initial results of the active compensation mode, which strongly suppresses the signal from surgical instruments placed near the detector.

Separation of excitation and detection coils

Then, we look into another challenge in **chapter 3**: can we downsize the detection system, such that it fits in a standard 6mm trocar opening, for laparoscopic detection of sentinel lymph nodes. The only way we can achieve this, and improve the maximum attainable detection depth, is by separating the excitation coil system from the detection coils. Usually, this is impossible, because the constantly varying mutual induction between the two coil sets is indistinguishable from the signal of interest, that of the particles. But because of the stepwise pulse sequence in DiffMag, we can allow for some measurement time to compensate for this changing mutual induction, as long as the rate of change of the mutual inductance is slow compared to the pulse sequence time.

Building on the DiffMag foundations laid in chapter 2, we elaborate on the phase sensitive detection scheme, and how it is used to calculate the optimal compensation signal which is coupled into the coils of the gradiometer. We then illustrate the physical setup, and the expanded electronics package, as the induction of the excitation coils is now such that two separate power amplifiers are required, one for the AC signal and one for the DC pulses. Following this description, we show the first results of the active, iterative compensation and finish by discussing improvements that are needed before this setup is ready for (pre)clinical evaluation in a controlled setting.

Modelling magnetic nanoparticles

When looking for an optimal combination of magnetic probes and tracers, it is essential to understand the physics underlying the tracerś behavior in the relevant field regime. These dynamics are primarily governed by the time-dependent evolution of sampleś magnetization due to externally applied magnetic fields. Especially in the magnetic field and frequency range where Neèl and Brownian relaxation mechanisms compete, a complete understanding of the physics involved is still lacking. In this chapter, we explored a model in which we propose a very basic coupling of both magnetization channels, through the effect that magnetic anisotropy has on the Neèl relaxation mechanism. The basic idea is that Brownian relaxation, even in the situation where Neèl relaxation dominates, acts to align the magnetic easy axis with the applied field, which shortens the Neèl relaxation time. We describe this model in **chapter 4**.

We explore the feasibility of this model by numerically evaluating the Fokker-Planck equations that describe both relaxation mechanisms, whilst taking into account the particle size and anisotropy distribution. The model was evaluated for three different particles, with overall good agreement between measurement and simulation.

Magnetic measurements were performed using the in house built *SuperParamagnetic Quantifier*, which is a coaxial magnetometry setup similar to those used in AC magnetometry experiments, but using the DiffMag excitation and detection scheme. In the chapter, we describe experimental parameters used in the experiment, and characterization of the samples, to which we added TEM images for size distribution measurmements.

Finally, we combine the discussion points from the individual chapters, and have a short outlook on the potential of DiffMag for clinical applications, and illustrate the steps that need to be taken before (pre)clinical evaluation can take place.

Samenvatting

De implementatie van magnetische detectietechnieken in de kliniek heeft lang achtergelopen bij ontwikkelingen in de samenleving in het algemeen. Hoewel technieken als MRI en (in mindere mate) MEG en MCG hun weg naar de kliniek hebben weten te vinden, is het gebruik van magnetische technieken voor diagnostiek en behandeling altijd beperkt gebleven tot goed gecontroleerde, afgeschermde omgevingen. In dit proefschrift beschijf ik de ontwikkeling van een gevoelige en selectieve methode om magnetische nanodeeltjes te gebruiken voor diagnostiek en lokalisatie, zonder de noodzaak voor afgeschermde omgevingen. Dit opent de deur naar een wereld vol nieuwe toepassingen voor magnetische detectie, variërend van intraoperatieve detectie van poortwachter lymfeklieren tot het volgen en lokaliseren van stamcelbehandelingen, en navigatietoepassingen.

Differential Magnetometry

In **Hoofdstuk 2** introduceer ik het concept van Differentiële Magnetometrie of DiffMag. Door een specimen die superparamagnetische ijzeroxide nanodeeltjes (SPIONs) te exciteren met een inductiespoel die een wisselend magneetveld genereert, magnetiseren we de deeltjes. Deze (alternerende) magnetisatie wordt gemeten met een gradiometer. Als we nu periodiek een statisch magneetveld toevoegen aan de excitatie, veranderen we de magnetische respons van de deeltjes, omdat de magnetisatie-dynamica van deze deeltjes sterk niet-lineair is. Als we nu het verschil tussen deze twee magnetisatiesignalen bepalen, verkrijgen we een specifiek signaal wat alleen van de deeltjes afkomstig kan zijn, wat contrasteert met het grotendeels lineaire magnetische gedrag van weefsel en chirurgisch instrumentarium in dit veldbereik. In dit hoofdstuk illustreren we hoe de tijdsafgeleide van de magnetisatie verandert wanneer de magnetisatie richting verzadiging wordt gebracht door het aangelegde statische offsetveld.

Het principe van DiffMag was geïmplementeerd in een draagbare sensor, bedoeld voor de intraoperatieve detectie van de poortwachter lymfeklier tijdens borstkankerchirurgie. Deze toepassing vormt een forse uitdaging voor magnetische technieken, omdat de eisen ten aanzien van gevoeligheid en selectiviteit hoog zijn, en de geïnjecteerde dosis zo laag mogelijk moet zijn om post-operatieve bijwerkingen als huidverkleuring en MRI artefacten te voorkomen. Daar komt bij dat het uitgestraalde vermogen van de spoelen beperkt is om weefselopwarming en andere effecten zoals beschreven in de *ICNIRP guidelines on non ionizing radiation* te voorkomen. Terwijl conventionele magnetometers, die verkend worden voor dit soort toepassingen, problemen hebben met het compenseren van het effect van een veranderende achtergrondsusceptibiliteit (bijvoorbeeld door veranderende zuurstofopname in het weefsel, wat dit licht paramagnetisch maakt) en metallisch chirurgisch instrumentarium, is DiffMag zeer robuust tegen dit soort arttefacten, als de meetelectronica snel genoeg is om in real time te compenseren voor het geïnduceerde ruissignaal. In dit hoofdstuk benoemen we de klinische eisen voor deze toepassing, en beschrijven we hoe deze vertaald zijn in het eerste prototype.

De sensor bestaat uit coaxiale paren excitatie- en detectiespoelen, met kleine compensatiespoelen hier omheen gewikkeld, zodat het magnetische signaal in real time bijgestuurd kan worden. De excitatiespoelen worden aangedreven door een stroomgestuurde voeding, die door middel van een data acquisitiesysteem aangestuurd wordt met MATLAB. Na de detectiespoelen volgt een eerste voorversterker met lage ruis als laatste onderdeel van de sensor. En gevoelige instrumentatieversterker ontvangt het signaal van de voorversterker en voert dit het data acquisitiesysteem in, waarna DiffMag signaalanalyse en verwerking worden uitgevoerd in MATLAB. Alle karakterisatiemetingen werden gedaan met samples van het bekende MRI contrastmateriaal *Resovist*. De werking van de sensor werd geverifieerd door middel van het meten van de dose-response curve, axiale en dieptegevoeligheid van de probe. Vervolgens laten we de eerste resultaten zien van het actieve compensatiemechanisme, wat het signaal van chirurgisch instrumentarium in de nabijheid van de probe sterk onderdrukt.

Separation of excitation and detection coils

Vervolgens bekijken we in **Hoofdstuk 3** een volgende uitdaging: het reduceren van de omvang van de sensor, zodat deze in een standaard 6mm trocar-opening past, zodat laparoscopische toepassingen binnen bereik komen. De enige manier waarop dit gerealiseerd kan worden, alsmede de dieptegevoeligheid van de sensor te verbeteren, is door de excitatiespoelen fysiek te scheiden van de detector. Normaliter is dit onmogelijk, aangezien de constant variërende mutuele inductie tussen excitatie en detectie niet te onderscheiden is van het signaal waar we in geïnteresseerd zijn. Vanwege de stapsgewijze veldsequentie van DiffMag kunnen we wat meettijd investeren om voor deze veranderende mutuele inductie te compenseren, zo lang de tijdsconstante van de verandering lang is ten opzichte van de meetsnelheid van ons systeem.

Voortbordurend op de DiffMag basisprincipes uit hoofdstuk 2, illustreren we het fasegevoelige detectie-algoritme, en hoe dit wordt gebruikt om het optimale compensatiesignaal te bepalen wat uiteindelijk door de compensatiespoelen in het systeem gekoppeld wordt. Vervolgens beschrijven we de fysieke opstelling en de electronica die uitgebreid is ten opzichte van het eerste prototype, aangezien we door de omvang van de excitatiespoelen nu twee stroomgestuurde voedingen moeten gebruiken, een voor het AC signaal en een voor het DC signaal. Hierna laten we de resultaten van de actieve compensatie zien, en sluiten af met het bediscussiëren van verbeteringen die nodig zijn voordat het systeem klaar is voor (pre)klinische evaluatie.

Modelling magnetic nanoparticles

Wanneer een optimale combinatie van magnetische sensor en deeltje gezocht wordt, is het essentieel om de natuurkunde te begrijpen die het magnetisch gedrag van de deeltjes in het relevante veldregime beschrijft. Dit gedrag wordt voornamelijk bepaald door de tijdafhankelijke ontwikkeling van de magnetisatie van het sample, veroorzaakt door het aangelegde excitatieveld. Juist in het gebied waar de Neèl en Brownse relaxatiemechanismes beide actief zijn, ontbreekt een complete beschrijving van de fysica. In dit hoofdstuk verkenden we een model waarin we een eenvoudige koppeling tussen beide relaxatiemechanismes voorstellen, door het effect wat magnetische anisotropie heeft op het Neèl mechanisme. Het idee is dat de Brownse beweging, zelfs in de situatie waar Neèl relaxatie normaliter domineert, de magnetische as van het deeltje dusdanig uitlijnt met het aangelegde magneetveld, dat daardoor de Neèl relaxatietijd verkort wordt. Ik beschrijf dit model in **Hoofdstuk 4**.

We bekijken de geschiktheid van dit model door numeriek de Fokker-Planckvergelijkingen die beide relaxatiemechanismes beschrijven te evalueren, terwijl we daarin de distributie van deeltjesgrootte en -anisotropie meenemen. Het model is geëvalueerd met drie verschillende types deeltjes, met goede overeenkomst tussen meting en model.

Magnetische metingen zijn uitgevoerd met de zelfgebouwde *Super-Paramagnetic Quantifier*, een coaxiale magnetometer vergelijkbaar met opstellingen die gebruikt worden om AC magnetometrie-experimenten uit te voeren, maar met DiffMag excitatie en detectiesequenties. In dit hoofdstuk beschrijven we de experimentele parameters van het experiment en karakterisatie van de samples, waar TEM microscopie gebruikt werd voor het bepalen van de grootte-distributie.

Tenslotte combineren we de discussiepunten van de individuele hoofdstukken, en kijken we vooruit naar potentiële toepassingen voor DiffMag in de kliniek, met een illustratie van de stappen die nog genomen moeten worden voordat (pre)klinische evaluatie kan plaatsvinden.

Acknowledgments

Dit boekje vormt dan uiteindelijk de afsluiting van een mooi en leerzaam traject. Een project waar ik veel in geïnvesteerd heb, maar wat mij ook enorm veel gegeven heeft. Het afsluiten van dit hoofdstuk betekent voor mij ook een punt zetten achter een periode met daarin zowel absolute hoogtepunten als zeker ook mindere periodes. Ik geloof intens dat samenwerken de sleutel tot succes is, zowel in de persoonlijke als professionele context, en wil de laatste woorden van dit proefschrift dan ook besteden aan het bedanken van de grote hoeveelheid mensen die mij naar de eindstreep hebben geholpen.

Als allereerste, mijn begeleider en promotor, Bennie ten Haken. We hebben in een behoorlijke achtbaan gezeten de laatste jaren, en ik ben je erg dankbaar voor alle steun, inspiratie en het vertrouwen wat ik altijd heb gevoeld, ook als ik dat zelf eigenlijk niet zo had. Tijdens dit traject heb ik mijzelf veel verder weten te ontwikkelen dan een 'standaard' PhD programma zou toestaan. De ruimte die je bood om mijn eigen pad te volgen, beslissingen te nemen waardeer ik meer dan ik kan opschrijven. Bedankt voor je onverwoestbare positiviteit. Ten tweede, het onderzoek wat ik in dit boek beschrijf zou niet mogelijk zijn geweest zonder de gouden handen van Erik Krooshoop. Bijna alles wat ik weet van electronica en spoelontwerp heb ik geleerd door met Erik te werken. In de laatste periode heb ik veel te danken gehad aan de steun van Lejla Alic, mijn co-promotor. Dank voor je kritische houding en energie.

Mijn twee paranimfen, Marcel en Wander, dank voor jullie steun en inspiratie, zowel binnen als buiten het werk. Ik prijs me gelukkig dat jullie me bijstaan tijdens de verdediging van dit proefschrift.

I'm very grateful for the opportunity to have such an amazing committee of opponents to spar with during my defense. Thank you for taking the time out of your busy schedules to assess my manuscript. A special word of thanks to the international members of my committee, prof. Conolly and prof. Ludwig. I've really appreciated our interactions during the various MPI Workshops, and have learned

a lot from your experience, knowledge and collaborative attitude. Thank you.

De basis van deze thesis werd gelegd in het *Arthur*-project, waarin de UT samenwerkte in een consortia met absolute experts in hun veld. Ik dank prof. dr. Joost Klaase, toen verbonden aan het MST in Enschede, nu hoogleraar aan het UMCG in Groningen, die mij kennis liet maken met chirurgische procedures, en wiens constante focus op het verbeteren van de kwaliteit van leven voor patiënten een echte inspiratiebron was voor mij als naïeve natuurkundige. Een tweede researchlijn met Kryoz Technologies (nu onderdeel van Demcon) leverde geen resultaten op die opgenomen zijn in dit proefschrift, maar ik heb veel geleerd van de thermodynamische expertise van Erik-Jan en Pieter-Paul. Céline Joosten en Patrick Meutstege van Panton waren als ontwerpers essentieel voor het ontwerpen van een probe die daadwerkelijk gebruikt zou worden door een arts, en de input van Rob Stemerdink (DKMS) en prof. dr. Jurgen Fütterer (Radboudumc) maakten het plaatje compleet. Dank jullie allen.

Every year at the IWMPI workshop, I've discussed with a group of scientists, and in a few cases this lead to a fruitful collaboration. Many thanks to Amit Khandhar and Matthew Ferguson of Lodespin Labs and professor Kannan Krishnan from the University of Washington. Our discussions have been a major influence in developing the particle models I describe in this thesis, and your generous supply of optimized magnetic nanoparticles made much of the experimental verification of these models possible.

Ik heb het grote geluk gehad te belanden in een onderzoeksgroep met een zeer diverse samenstelling: biomedisch technologen, technisch geneeskundigen en natuurkundigen. Ik heb erg genoten van alle koffie- en lunchpauzes met mijn collega PhD kandidaten: Bas-Jan, Joost, Kirsten, Martijn, Marleen en Sofie. In de laatste jaren kwamen daar Lennert, Eliane en in het bijzonder Melissa bij, die verder bouwden op de basis die gelegd was voor DiffMag, wat fantastisch is om te zien. Dank ook aan de verschillende secretaresses van de vakgroep die, zoals iedere wetenschapper weet, eigenlijk de groep draaiende houden. Dankjewel Esmeralda, Jolanda, Tanja en Titia. Een speciaal woord van dank voor mijn allereerste afstudeer-student en direct daarna collega Tasio. Samen met jou aan DiffMag werken was echt heel mooi.

Een van de mooiste aspecten van dit PhD project voor mij was het begeleiden van bachelor- en masterstudenten. Ik had het geluk met een lange lijst studenten te mogen werken, en ik ben er van overtuigd dat jullie delen van je werk zullen herkennen in dit proefschrift. Dankjewel Aline, Anneloes, Bart, Friso, Kevin, Kimberley, Maaike, Max, Paul, Rogier, Suzan, Eline, Lydia, Moniek en Kay.

Toen mijn onderzoek bijna klaar was, kreeg ik de unieke kans om onderdeel te worden van wat we nu kennen als het TechMed Centre. Het is schitterend om te zien hoe ons kleine team van toen inmiddels uitgegroeid is tot een absoluut topinstituut met dito infrastructuur, en ik werk met heel veel plezier samen met mijn collega's van TechMed Office, Research en Academy. Het bouwen aan het TechMed Centre, zowel als organisatie als het fysieke gebouw is een fantastisch avontuur, en ik wil vooral Remke bedanken voor de vrijheid en het vertrouwen om mijn werk zodanig in te richten dat ik dit proefschrift kon afronden. En natuurlijk, 'mijn' team binnen TechMed Infra: jullie zijn het mooiste team om voor te mogen werken, en ik ben trots op wat we samen neergezet hebben. Dank voor jullie vertrouwen en steun.

Een speciale dank voor de UT collega's met wie ik ervaringen heb kunnen delen tijdens de leiderschapstrajecten die ik heb mogen volgen. Toen ik aan mijn Master Technische Natuurkunde begon, werd mijn enthousiasme voor wetenschap gevoed en aangewakkerd door mijn uiteindelijke afstudeerhoogleraren, prof. Alexander Brinkman en prof. Hans Hilgenkamp. Vooral Hans ben ik zeer erkentelijk voor zijn steun tijdens een bijzonder moeilijke periode. Dank voor jullie inspiratie en support.

There's more to life than work alone. Dank aan al mijn studievrienden, fietsvrienden, houtdraai-vrienden die mij helpen om m'n kop recht op m'n schouders te houden. Hoewel mijn werk misschien wat ongrijpbaar is voor veel (schoon)familie, is hun steun me zeer dierbaar. Mijn basis werd gelegd in Zwolle, door mijn ouders en zusje, die me altijd hebben vertrouwd in mijn keuzes. Dank voor jullie nooit aflatende steun, zeker in moeilijke periodes, en voor het vormen van mijn fundament.

Aan het begin van dit proefschrift waren we met z'n tweeën, nu zijn er vier, plus Kyra. Ik weet behoorlijk zeker dat ik hier niet had gestaan zonder mijn fantastische en sterke vrouw, en schitterende kinderen. Janneke, dank je wel voor je liefde, je steun en je begrip voor mijn atypische brein. Elise en Matthijs: met jullie is iedere dag een feestje. Ik kan niet wachten om de wereld met jullie te verkennen en samen te blijven groeien.

-sebastiaan

Scientific output

Articles

1. M. Visscher, **S. Waanders**, H.J.G. Krooshoop, B. ten Haken, Selective detection of magnetic nanoparticles in biomedical applications using differential magnetometry, *Journal of Magnetism and Magnetic Materials* 365:31-39, 2014.

2. M. Visscher, **S. Waanders**, J.J. Pouw, B. ten Haken, Depth limitations for in vivo magnetic nanoparticle detection with a compact handheld device, *Journal of Magnetism and Magnetic Materials* 380:246-250, 2015.

3. **S. Waanders**, M. Visscher, R.R. Wildeboer, T.O.B. Oderkerk, H.J.G. Krooshoop, B. ten Haken, A handheld SPIO-based sentinel lymph node mapping device using differential magnetometry, *Physics in Medicine and Biology* 61(22), 2016.

4. M.M. Horstman - van de Loosdrecht, **S. Waanders**, H.J.G. Krooshoop, B. ten Haken, Separation of excitation and detection coils for in vivo detection of superparamagnetic iron oxide nanoparticles, *Journal of Magnetism and Magnetic Materials* 475:563-569 (2019)

5. M.M. Horstman - van de Loosdrecht, S. Draack, **S. Waanders**, J.G.L. Schlief, H.J.G. Krooshoop, T. Viereck, F. Ludwig, B. ten Haken, A novel characterization technique for superparamagnetic iron oxide nanoparticles: The superparamagnetic quantifier, compared with magnetic particle spectroscopy, *Review of Scientific Instruments* 90(2), 2019.

6. M.T. Rietberg, **S. Waanders**, M.M. Horstman - van de Loosdrecht, R.R. Wildeboer, B. ten Haken, L. Alic, Modelling of dynamic behaviour in magnetic nanoparticles, *Nanomaterials* 11(12), 2021.[1]

[1] M.T. Rietberg and S. Waanders share first authorship on this article.

Patent

1. **S. Waanders**, M. Visscher, T.O.B. Oderkerk, H.J.G. Krooshoop, B. ten Haken, Method and apparatus for measuring an amount of superparamagnetic material in an object, EU Patent EP2923216B1, filed 19-11-2013, granted 28-09-2016.

Conference contributions

1. M. Visscher, **S. Waanders**, J.J. Pouw, H.J.G. Krooshoop, B. ten Haken, Ex vivo quantification of magnetic nanoparticles in clinical samples at room temperature with high specificity and improved stability (poster), 9th International Conference on the Scientific and Clinical Applications of Magnetic Carriers, Minneapolis (USA), 2012.
2. P. van Kaam, E.B. van Dieren, **S. Waanders**, B. ten Haken, Use of magnetic nano particles for localisation in radiotherapy (poster), Wetenschapssymposium MST, Enschede, 2012.
3. **S. Waanders**, M. Visscher, T.O.B. Oderkerk, B, ten Haken, Finding the sentinel lymph node with a Differential Magnetometer (oral), 3rd International Workshop on Magnetic Particle Imaging, Berkeley (USA), 2013.
4. M. Visscher, **S. Waanders**, B, ten Haken, Analyzing magnetic nanoparticle content in biological samples: AC susceptometry using offset fields (oral), 3rd International Workshop on Magnetic Particle Imaging, Berkeley (USA), 2013.
5. **S. Waanders**, T.O.B. Oderkerk, M. Visscher, H.J.G. Krooshoop, B. ten Haken, Handheld Differential Magnetometry with a split coil geometry (oral), 4th International Workshop on Magnetic Particle Imaging, Lübeck (Germany), 2014.
6. M. Visscher, **S. Waanders**, J.J. Pouw, B. ten Haken, Depth limitations for in vivo magnetic nanoparticle detection with a handheld device (oral), 10th International Conference on the Scientific and Clinical Applications of Magnetic Carriers, Dresden (Germany), 2014.
7. **S. Waanders**, M. Ahmed, B. Anninga, R.M. Ferguson, A.P. Khandhar, S. Kemp, M. Douek, K.M. Krishnan, B. ten Haken, SPIO requirements for in vivo sentinel lymph node localization (oral), 5th International Workshop on Magnetic Particle Imaging, Istanbul (Turkey), 2015.
8. M.M. Horstman - van de Loosdrecht, **S. Waanders**, R.R. Wildeboer, H.J.G. Krooshoop, B. ten Haken, Differential Magnetometry to detect sentinel lymph nodes in laparoscopic procedures (poster), 7th International Workshop on Magnetic Particle Imaging, Prague (Czech Republic), 2017.
9. M.M. Horstman - van de Loosdrecht, S. Draack, **S. Waanders**, H.J.G. Krooshoop, F. Ludwig, B. ten Haken, Comparison of Superparamagnetic Quantifier and Magnetic Particle Spectroscopy (poster), 8th International Workshop on Magnetic Particle Imaging, Hamburg (Germany), 2018.

10. M.M. Horstman - van de Loosdrecht, **S. Waanders**, H.J.G. Krooshoop, B. ten Haken, Characterization of superparamagnetic iron oxide nanoparticles in biological environments (poster), 12th International Conference on the Scientific and Clinical Applications of Magnetic Carriers, Copenhagen (Denmark), 2018.
11. M.M. Horstman - van de Loosdrecht, **S. Waanders**, H.J.G. Krooshoop, B. ten Haken, Differential Magnetometry to detect sentinel lymph nodes in laparoscopic procedures: static results (poster), 12th International Conference on the Scientific and Clinical Applications of Magnetic Carriers, Copenhagen (Denmark), 2018.
12. M.M. Horstman - van de Loosdrecht, **S. Waanders**, H.J.G. Krooshoop, B. ten Haken, Separation of excitation and detection coils to locate superparamagnetic iron oxide nanoparticles in vivo (oral), 9th Joint European Magnetic Symposia, Mainz (Germany), 2018.
13. M.M. Horstman - van de Loosdrecht, **S. Waanders**, H.J.G. Krooshoop, B. ten Haken, Laparoscopic sentinel node biopsy using Differential Magnetometry (poster), 7th Dutch Bio-Medical Engineering Conference, Egmond aan Zee (Netherlands), 2019.